2004

Mesozoic-Cenozoic evolution of the Xining-Minhe and Dangchang basins, northeastern Tibetan Plateau: Magnetostratigraphic and biostratigraphic results

B. K. Horton

Guillaume Dupont-Nivet

J. Zhou

G. L. Waanders

Robert F. Butler
University of Portland, butler@up.edu

See next page for additional authors

Mesozoic-Cenozoic evolution of the Xining-Minhe and Dangchang basins, northeastern Tibetan Plateau: Magnetostratigraphic and biostratigraphic results

B. K. Horton,[1] G. Dupont-Nivet,[1,2] J. Zhou,[3] G. L. Waanders,[4] R. F. Butler,[5] and J. Wang[6]

Received 26 November 2003; revised 6 December 2003; accepted 24 December 2003; published 1 April 2004.

[1] Accurate stratigraphic ages are crucial to understanding the deformation history of the Tibetan Plateau prior to and during the Indo-Asian collision. Efforts to quantify Mesozoic-Cenozoic ages are hindered by limited fossils and a paucity of volcanic horizons and regionally correlative strata. Magnetostratigraphic and biostratigraphic results from the Xining-Minhe-Longzhong basin complex and Dangchang basin provide an improved chronology of nonmarine basin development over a large region of the northeastern Tibetan Plateau (34–37°N, 101–105°E). Analyses of 171 magnetostratigraphic levels and 24 palynological assemblages (>120 species) indicate Late Jurassic-Early Cretaceous to mid-Tertiary deposition. Although magnetic polarity zonation is incomplete, independent palynological age control partially restricts possible correlations to the Geomagnetic Polarity Timescale. The sediment accumulation record, basin provenance, structural geology, and published thermochronological data support a history of Jurassic exhumation, Late Jurassic-Early Cretaceous fault-related basin initiation, and Cretaceous-Paleogene reduced accumulation. These patterns, which are compatible with Late Jurassic-Early Cretaceous extension and Cretaceous-Paleogene postrift thermal subsidence, were disrupted at about 40–30 Ma, when shortening related to the Indo-Asian collision induced localized range uplift, vertical axis rotation, and amplified subsidence. *INDEX TERMS:* 1520 Geomagnetism and Paleomagnetism: Magnetostratigraphy; 8102 Tectonophysics: Continental contractional orogenic belts; 9320 Information Related to Geographic Region: Asia; 9604 Information Related to Geologic Time: Cenozoic; 9609 Information Related to Geologic Time: Mesozoic; *KEYWORDS:* tectonics, magnetostratigraphy, Tibetan Plateau, Cenozoic, Mesozoic, sedimentary basins

Citation: Horton, B. K., G. Dupont-Nivet, J. Zhou, G. L. Waanders, R. F. Butler, and J. Wang (2004), Mesozoic-Cenozoic evolution of the Xining-Minhe and Dangchang basins, northeastern Tibetan Plateau: Magnetostratigraphic and biostratigraphic results, *J. Geophys. Res.*, *109*, B04402, doi:10.1029/2003JB002913.

1. Introduction

[2] Resolving the timing of deformation across the Tibetan Plateau is fundamental to addressing models of plateau construction. Although many studies highlight the importance of the Indo-Asian collision in driving middle to late Cenozoic deformation [e.g., *Molnar and Tapponnier*, 1975; *Dewey et al.*, 1988; *Burchfiel and Royden*, 1991; *DeCelles et al.*, 2002], substantial Mesozoic to early Cenozoic deformation may have affected large areas of the Tibetan Plateau [*Burg and Chen*, 1984; *Murphy et al.*, 1997; *Yin and Harrison*, 2000; *Horton et al.*, 2002; *Kapp et al.*, 2003]. Long-term stratigraphic chronologies for Mesozoic-Cenozoic successions are vital for ascertaining the timing, distribution, and possible northward progression of deformation that preceded and accompanied the Indo-Asian collision.

[3] Obstacles to chronological studies in the Tibetan Plateau include a shortage of diagnostic fossils, pronounced lithostratigraphic similarities (precluding unique regional correlations), and limited volcanic horizons in Upper Jurassic–Tertiary strata [*Kidd et al.*, 1988; *Yin et al.*, 1988]. Although marine strata are reported in places [*Zhang*, 2000] and important mammal fossils characterize some Neogene deposits [*Qiu et al.*, 2001; *Wang et al.*, 2003], most mid-Mesozoic through Cenozoic sedimentary rocks consist of nonfossiliferous, oxidized red beds of fluviolacustrine origin. Because of the scarcity of published age constraints, several regional studies rely exclusively on age interpretations from regional Chinese mapping efforts

[1]Department of Earth and Space Sciences, University of California, Los Angeles, California, USA.
[2]Now at Faculty of Earth Sciences, Paleomagnetic Laboratory "Fort Hoofdijk", Utrecht University, Utrecht, Netherlands.
[3]Faculty of Earth Sciences, China University of Geosciences, Wuhan, China.
[4]Waanders Palynology, Encinitas, California, USA.
[5]Department of Geosciences, University of Arizona, Tucson, Arizona, USA.
[6]Institute of Geochemistry, Chinese Academy of Sciences, Guangzhou, China.

0148-0227/04/2003JB002913$09.00

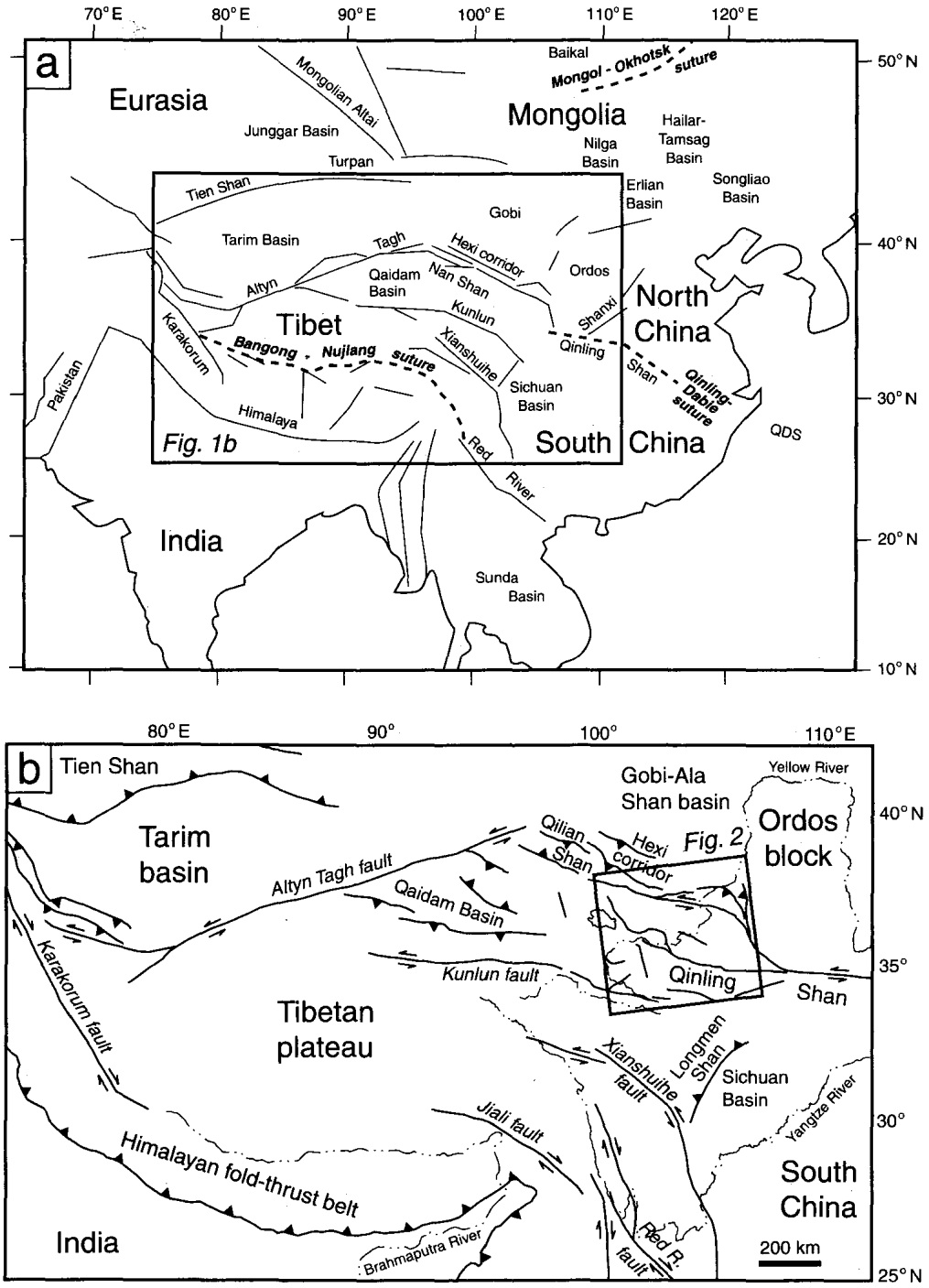

Figure 1. (a) Regional tectonic map of east Asia. (b) Map of the Tibetan Plateau and adjacent regions showing principal active faults, sedimentary basins, and rivers.

[e.g., *Halim et al.*, 1998; *Métivier et al.*, 1998; *Cogné et al.*, 1999]. In many cases, however, the rationale behind these age interpretations and regional correlations, as well as the original sample locations and stratigraphic levels, remain unspecified in the available literature. Furthermore, in some instances, dating of volcanic horizons reveals discrepancies with original map-assigned ages on the order of 20–80 Myr [e.g., *Horton et al.*, 2002; *Kapp et al.*, 2002].

[4] The purpose of this paper is to develop a chronological framework on the basis of magnetostratigraphy and palynological biostratigraphy to evaluate late Mesozoic to mid-Tertiary basin evolution and sediment accumulation patterns in the northeastern Tibetan Plateau (Figure 1). These chronostratigraphic techniques may provide the best clues to distinguishing Mesozoic rocks from lithologically similar Cenozoic rocks in other parts of the Tibetan plateau. In the companion paper, *Dupont-Nivet et al.* [2004] address tectonic rotations revealed by the paleomagnetic analyses.

2. Geologic Setting

[5] The northeastern corner of the Tibetan Plateau constitutes the region bounded by the Qinling Shan and

Kunlun fault to the south, Qilian-Nan Shan to the west-northwest, and Haiyuan fault and Liupan Shan to the north and east (Figure 2). Narrow, 3000- to 4500-m-high ranges produced by Cenozoic shortening and strike-slip deformation separate adjacent basins situated at 1500–3000 m [*Tapponnier et al.*, 1990; *Zhang et al.*, 1990, 1991; *Burchfiel et al.*, 1991; *Gaudemer et al.*, 1995; *Meyer et al.*, 1998; *Lasserre et al.*, 2002]. Rather than an abrupt plateau margin, a uniform decrease in elevation from southwest to northeast [*Clark and Royden*, 2000] is expressed along the approximate trace of the Yellow River (Figure 2a). Average crustal thickness also decreases from southwest to northeast, from ~60 km near the Kunlun fault to ~40 km near the Haiyuan fault [*Galvé et al.*, 2002; *Zhang et al.*, 2002].

[6] Timing of surface uplift in the northern Tibetan Plateau remains poorly known. Although many infer Pliocene-Quaternary uplift on the basis of a regional conglomeratic influx since ~4 Ma [e.g., *Li*, 1995; *Li and Fang*, 1999; *Zheng et al.*, 2000], the distribution and apparent synchroneity of this textural variation may be more consistent with climate change [*Liu et al.*, 1996; *Zhang et al.*, 2001]. A growing body of thermochronological evidence, mainly fission track data, indicate Mesozoic-early Tertiary cooling episodes in northern Tibet [*Mock et al.*, 1999; *George et al.*, 2001; *Jolivet et al.*, 2001; *Sobel et al.*, 2001], consistent with sedimentation histories in northern Tibet [*Hanson*, 1999; *Yin et al.*, 2002] and possibly Cretaceous-early Tertiary deformation and uplift in the plateau interior [*Burg et al.*, 1983; *Burg and Chen*, 1984; *Allègre et al.*, 1984; *England and Searle*, 1986; *Pan*, 1993; *Murphy et al.*, 1997; *Yin and Harrison*, 2000; *Horton et al.*, 2002; *Kapp et al.*, 2003]. Nevertheless, occurrences of marine strata in northern Tibet and the Tarim basin [*Bally et al.*, 1986; *Watson et al.*, 1987; *Yin et al.*, 1988; *Sobel*, 1999; *Yin and Harrison*, 2000] suggest that some areas remained relatively low during Cretaceous-early Tertiary time.

[7] Sedimentation north of the Kunlun fault involved large Cenozoic basins such as the Qaidam, Tarim, Junggar, and Turpan basins (Figure 1), and their Mesozoic precursors [*Bally et al.*, 1986; *Hendrix et al.*, 1992; *Graham et al.*, 1993; *Métivier et al.*, 1998; *Sobel*, 1999; *Ritts and Biffi*, 2000]. Cenozoic accumulation recorded the flexural response to shortening-induced crustal thickening [*Bally et al.*, 1986; *Meyer et al.*, 1998; *Yin et al.*, 2002] and/or topographic isolation through closure of drainage outlets [*Métivier et al.*, 1998; *Tapponnier et al.*, 2001]. Similar mechanisms may apply to smaller Cenozoic basins in central and northern Tibet [e.g., *Leeder et al.*, 1988; *Liu et al.*, 2001; *Horton et al.*, 2002; *Pares et al.*, 2003]. In contrast, regional Mesozoic sedimentation in northern Tibet, north China, and Mongolia (Figure 1a) is variably attributed to (1) shortening and strike-slip deformation due to collisions along the Kunlun and Bangong-Nujiang sutures in central Tibet, (2) extension and strike-slip deformation linked to retreating subduction zones to the north and east (Mongol-Okhotsk and Pacific margins, respectively), and (3) extensional collapse of east trending mountain belts in north China and Mongolia [*Hsü*, 1989; *Xu et al.*, 1989; *Hendrix et al.*, 1992, 1996; *Graham et al.*, 1993, 2001; *Sobel*, 1999; *Vincent and Allen*, 1999; *Davis et al.*, 2001, 2002; *Ritts et al.*, 2001; *Darby and Ritts*, 2002; *Meng et al.*, 2003; *Robinson et al.*, 2003].

3. Stratigraphic Synthesis

3.1. Regional Overview

[8] A complex stratigraphic nomenclature characterizes Mesozoic-Cenozoic basins in the vicinity of Xining and Lanzhou, two cities near the Qinghai-Gansu provincial border (Figure 2). Most successions contain predominantly Cretaceous red clastic strata that persist laterally throughout the region and originally covered >30,000 km^2. An Upper Jurassic section concordantly underlies these rocks in places. The Jurassic-Cretaceous package is referred to as the Xining-Minhe basin or Minhe basin. The approximate outcrop extent (Figure 2) suggests an original southern basin margin south of the Laji Shan, eastern basin margin near the Maxian Shan (near Lanzhou), northern basin margin near the Qilian Shan (Daban Shan, locally), and western basin margin near the Qinghai Nan Shan. Lower Tertiary rocks that concordantly overlie Cretaceous strata in most of the Xining-Minhe basin have been traditionally considered part of a younger broader basin, the Longzhong basin [*Zhai and Cai*, 1984]. Nomenclature is further complicated by the delineation of four Cenozoic subbasins (the Xining, Lanzhou, Linxia and Longxi-Jingning subbasins) within the composite Longzhong basin (Figure 2b). For consistency with previous studies, the original names are retained here and the term Xining-Minhe-Longzhong basin complex is introduced to refer jointly to the Mesozoic Xining-Minhe basin and Cenozoic Longzhong basin. The Longzhong basin covered >100,000 km^2 between the Qinling Shan and Haiyuan fault during Cenozoic sedimentation (Figure 2). Paleogene strata are best preserved in the Xining subbasin and along the northern flank of the Qinling Shan. During Oligocene-Miocene time, deposition persisted in these areas and initiated in the Linxia and Lanzhou subbasins and a series of basins southwest of the Laji Shan: the Gonghe, Guide, and Xunhua basins (Figure 2b) [*Zhai and Cai*, 1984; *Li*, 1995; *Li et al.*, 1997a, 1997b; *Flynn et al.*, 1999; *Qiu et al.*, 2001; *Yue et al.*, 2001; *Pares et al.*, 2003; *Song et al.*, 2003]. Variability in basin nomenclature may reflect systematic partitioning of the original Mesozoic Xining-Minhe basin by Cenozoic uplift of narrow ranges.

3.2. Xining-Minhe-Longzhong Basin Complex and Dangchang Basin

[9] A synthesis of Jurassic-Miocene stratigraphy (Figures 3 and 4) based on this study and previous studies [*Qinghai Bureau of Geology and Mineral Resources* (*QBGMR*), 1985; *Zhai and Cai*, 1984; *Hao*, 1988; *Yu et al.*, 2001] lists the formations, lithologies, and age control from pollen, charophyte (algae), vertebrate (principally mammal), ostracod, conchostracan, bivalve, and gastropod fossils. Diagnostic fossils and age relationships are as follows.

[10] (1) Middle Jurassic Yaojie and Xiantang formations contain ostracod *Darwinula* and palynomorphs *Cyathidites*, *Deltoidospora*, *Classopollis*, and *Osmundacidites* [*QBGMR*, 1985; *Pang and Whatley*, 1990]. (2) Upper Jurassic Datonghe Formation contains ostracods *Damonella*, *Djungarica*, and *Minheella*, and charophytes *Aclistochara* and *Latochara*, similar to Late Jurassic assemblages of China, Mongolia,

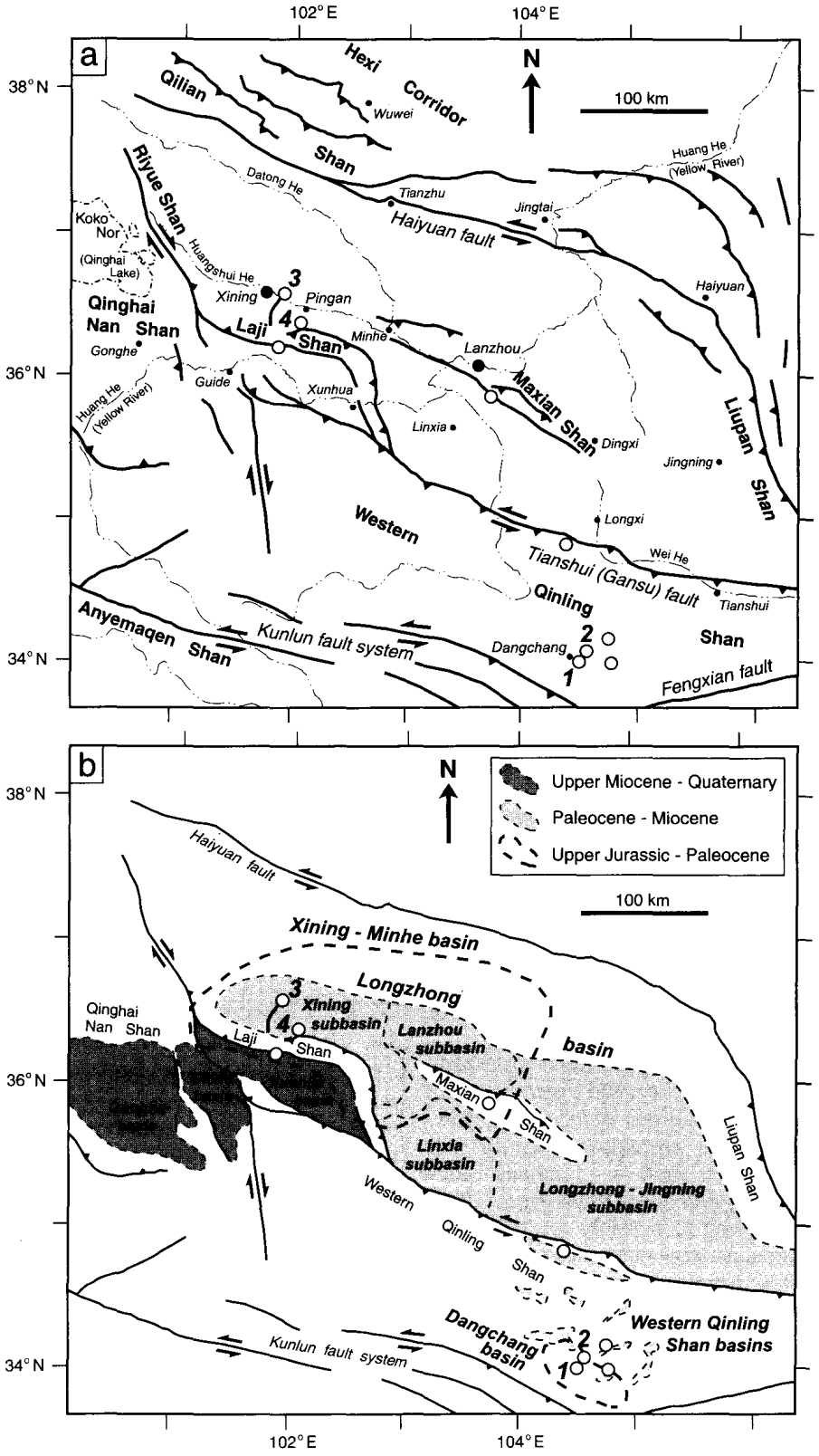

Figure 2. (a) Simplified tectonic map of the northeastern Tibetan Plateau showing the main thrust faults (barbed lines), strike-slip faults (arrows), mountain ranges, rivers, and cities. (b) Map of same region depicting approximate boundaries of Mesozoic-Cenozoic basin systems. Open circles denote locations of studied stratigraphic sections (1, south Dangchang; 2, north Dangchang; 3, east Xining; 4, Pingan).

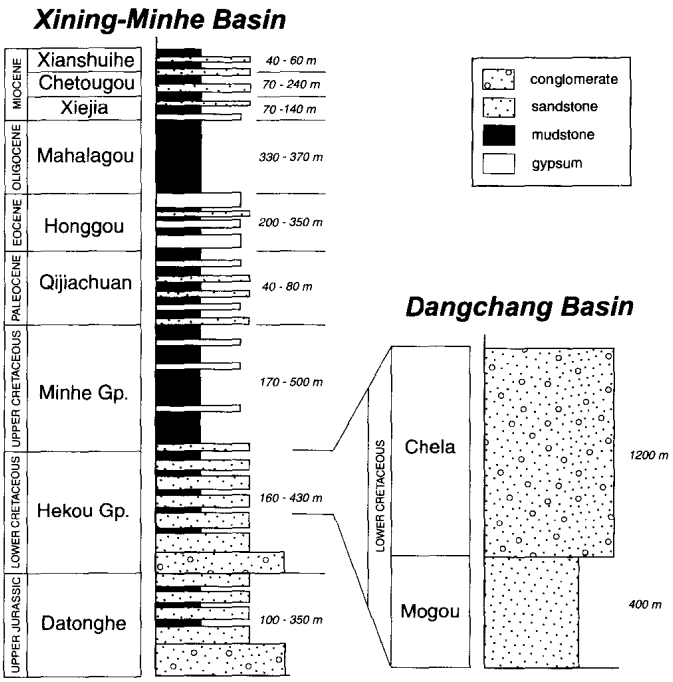

Figure 3. Generalized stratigraphic column listing formation names, lithologies, and thicknesses for the Xining-Minhe and Dangchang basins. See Figures 4 and 5 for detailed information.

and western United States [*Su et al.*, 1983; *Hao*, 1988; *Li*, 1988; *Pang and Whatley*, 1990]. (3) Lower Cretaceous Hekou Group contains ostracods *Cypridea*, *Lycopterocypris*, and *Ziziphocypris*, conchostracans *Eosestheria* and *Yanjiestheria*, charophytes *Aclistochara* and *Mesochara*, and palynomorphs *Cicatricosisporites*, *Schizaeoisporites*, *Classopollis*, *Piceaepollenites*, *Deltoidospora*, and *Cedripites*. The ostracods, charophytes, and conchostracans are common to abundant in Lower Cretaceous rocks of Eurasia and western United States [*Su et al.*, 1983; *Hao*, 1988; *Li*, 1988; *Pang and Whatley*, 1990; *QBGMR*, 1991; *Tang et al.*, 2001]. (4) Upper Cretaceous Minhe Group contains ostracods *Cristocypridea*, *Talicypridea*, *Cypridea*, and *Candona*, charophyte *Latochara*, and palynomorphs *Schizaeoisporites*, *Classopollis*, *Ephedripites*, and *Tricolporopollenites*. All are typical of Upper Cretaceous strata in China and Mongolia [*Su et al.*, 1983; *Zhai and Cai*, 1984; *Hao*, 1988; *QBGMR*, 1991]. (5) Paleocene to possibly lower Eocene Qijiachuan Formation contains large quantities of ostracods *Cypris* and *Limnocythere*, charophytes *Stephanochara*, *Harrisisichara*, *Peckichara*, and *Rhabdochara*, and palynomorphs *Ephedripites*, *Proteacidites*, *Scabiosapollenites*, and *Normapollis*, similar to upper Paleocene and possibly lower Eocene strata in China [*Zhai and Cai*, 1984; *Guan*, 1988; *Hao*, 1988; *QBGMR*, 1991]. (6) The Eocene Honggou Formation contains ostracods *Limnocythere*, *Ilyocypris*, and *Cyprinotus*, charophyte *Gyrogona* (the main component of middle to upper Eocene strata in China), and palynomorphs *Quercoidites*, *Celtis*, *Ulmipollenites*, and *Iodes* [*Zhai and Cai*, 1984; *Hao*, 1988; *He et al.*, 1988; *QBGMR*, 1991; *Liu and Yang*, 1999]. (7) Oligocene Mahalagou Formation contains a large appearance of ostracod *Ilyocypris*, additional ostracods *Cyprinotus* and *Eucypris*, charophytes *Maedlersphaera* and *Sphaerochara*, and palynomorphs *Meliaceoidites*, *Piceapollenites*, *Ephedripites*, and *Chenopodipollis*, common in Oligocene strata of Eurasia [*Zhai and Cai*, 1984; *Hao*, 1988; *QBGMR*, 1991; *Yu et al.*, 2001]. (8) Miocene Xiejia, Chetougou, and Xianshuihe formations are characterized by the appearance of a tremendous range of vertebrate fossils [*Zhai and Cai*, 1984] and the presence of ostracods *Eucypris* and *Ilyocypris*, charophytes *Charites*, and palynomorphs *Potamogeton*, *Quercoidites*, and *Gramineae* [*Zhai and Cai*, 1984; *Hao*, 1988; *QBGMR*, 1991; *Yu et al.*, 2001].

[11] In addition to fossil assemblages, Eocene-Oligocene marker horizons (gypsum beds in the Hongguo and Mahalagou formations) facilitate regional stratigraphic correlations. For example, a 5- to 30-m-thick gypsum in the upper Hongguo Formation can be traced >50 km, from local salt mines northwest of Xining to south of Pingan (Figure 2). This unit (E_2h^3) and similar units visible on aerial photograph and satellite imagery are located and described in previous maps and reports [*Zhai and Cai*, 1984; *QBGMR*, 1985].

3.3. Additional Palynological Age Control

[12] We present >120 palynological species identified in 24 samples from Jurassic-Tertiary strata (Tables A1 and A2[1]), adding to the ~80 previously reported species (Figure 4). For each sample, 5–10 grams of siltstone was dissolved in HCl and HF acids. Resistant pollen grains were sieved with 10 μm mesh, floated in a solution of $ZnBr_2$ (specific gravity of 2.0), mounted on standard slides, and examined using a binocular microscope. An additional 17 samples were barren of palynomorphs. Jurassic-Cretaceous palynological assemblages are dominated by gymnosperms and pteridophytes (ferns), with small proportions of angiosperms in Upper Cretaceous strata. Tertiary assemblages are dominated by angiosperms with small but regular occurrences of gymnosperm and pteridophytic flora. *Zhai and Cai* [1984] noted similar distributions in the Xining-Minhe basin.

3.4. Depositional Environments

[13] Jurassic-Tertiary strata are composed of lithofacies associations attributable to deposition in lacustrine and distal fluvial environments with subordinate proximal fluvial and alluvial fan environments. Comprehensive descriptions and interpretations, based on measured sections (Figure 5), are presented in Table A3.

[14] Lacustrine deposits, the volumetrically dominant facies, consist of thick intervals (100–1000 m) of thin-bedded, moderately well sorted, red, yellow, and variegated mudstone, sandstone, and minor evaporite. Deposition is attributed to suspension fallout and turbidity currents, with gypsum precipitation occurring during evaporative playa lake conditions, most notably during Eocene-Oligocene time.

[15] Overbank fluvial deposits are widespread, consisting of moderately thick intervals (20–200 m) of thin- to medium-bedded tan and red sandstone and interbedded mudstone. Clastic deposition is interpreted to be the result of crevasse splays and suspension fallout in an over-

[1]Auxiliary material is available at ftp://ftp.agu.org/apend/jb/2003JB002913.

Stratigraphy				Lithology	Fossils: 1—ostracod; 2—conchostracan; 3—charophyte (algae); 4—vertebrate (principally mammal); 5—pollen; 6—bivalve; 7—gastropod.
NEOGENE	MIOCENE	Xianshuihe	Xianshuihe Fm.[a]	Yellow calcareous mudstone with marl, sandstone, and sandy conglomerate	1: *Eucypris subovata, E. bella, E. magnifeca, E.* aff. *rischtanica* Schn., *Hemicyprinotus regularis, Cyclocypris xiningensis, C. umbellata, Ilyocypris sublevis*. 3: *Maedlerisphaera chinensis*. 4: *Gomphotherium connexus, G. wimani, Platybelodon grangeri, Plesiodipus leei, Oioceros noverca, Alloptox chinghaiensis, Bunolistriodon minheensis, Listriodon gigas, Stephanocemas chingaiensis, Elasmotherini, Micromeryx* sp.
		Chetougou		Yellow calcareous siltstone with gypsiferous sandstone, and pebbly sandstone	1: *Eucypris flexilis, E. magna, E. subovata, E. magnifeca, E.* aff. *rischtanica* Schn., *Hemicyprinotus regularis, Cyprinotus callicomus, C. gemmiformis, Cyclocypris xiningensis, C. ambellata, Candoniella marteida, Ilyocypris cornae, I. dushanensis, Limnocythere faceta*. 3: *Charites* cf. *chaidamuensis* (S. Wang), *Ch. parvula, Sphaerochara* cf. *granulifera* (Heer), *Maedlerisphaera chinensis, Hamichara kasakstanica*. 4: *Megacricetodon sinensis, M.*cf. *sinensis, Eumyarion* sp., *Protalactaga tunggurensis*, Rhinocerotidae, Cervidae, *Hispanotherium* sp., *Aceratherium* sp., *Plesiaceratherium* sp., *Heterosminthes orientalis, Palaeomeryx* sp., *Sinomicceros, Stephanocemas* sp. 5: *Quercoidites, Ulmipollenites, Gramineae, Inaperturopollenites, Schizosporites*.
		Xiejia Fm.		Red-brown calcareous silty mudstone interbedded with gypsiferous mudstone and pebble-sandstone	1: *Limnocythere sp., L. faceta, Ilyocypris* sp., *I. bradyi, I. sublevis, I. gibba, I. errabundis, Eucypris* sp., *Cyprinotus icrobus, C. xiningensis*. 3: *Charites minutissima, C. rarvula, Raskyaechara* (?), *Sphaerochara granulifera*. 4: Cricetidae (? cf. *Eumyarion* sp.), *Sinolagomys* sp., *S. pachygnathus, S.* cf. *pachygnathus, Leporidae* indet., *Sciurus* sp., *Otoceros* sp., *Eucricetodon* youngi, *Plesiosminthus xiningensis, P. huangshuiensis, P. lajeensis, Tataromys* sp., cf. *Tataromys* sp., *Tataromys suni, Tachyoryctoides kokonorensis, Cricetodon* sp., Mustelidae indet., *Brachypotherium* sp., *Oioceros xiejiaensis, Carnivora* indet., *Ctenopharyngodon* sp., *Ctenodyctylidae* indet., *Aflantoxerus, Diacerartherium* sp., *Sinopalaeoceros xiejiaensis*. 5: *Piceapollenites, Ulmipollenites, Quercoidites, Chenopodipollis, Labitricolpites, Meliaceoidites, Potamogeton, Sparganiacaepollenites*.
PALEOGENE	OLIGOCENE	Mahalagou Fm.	Upper Xining Gp.[a]	Red calcareous silty mudstone, gray gypsiferous mudstone.	1: *Cyprinotus* sp., *C. xiningensis, C. icrobus, C. dongyaomiaoensis, C. jucundus, C. gregarius, C. norini, C. subtriangulus, C. ensilada, C. arasensis, C.* aff. *qiuxianensis* Lee, *Eucypris* sp., *E. cavernosa, E. milagouensis, E. koktalensis, E.*cf. *E concinna* Schn., *Cypridopsis* cf. *reniformis, Cypris trigono, Ilyocypris* sp., *I. errabundis, I. suberrabundis, I. bradyi, I. sublevis, I. ellipsoidea, I. costata, I. manasensis confrogosa, Limnocythere linguida, Limnocythere* cf. *emarciara, Limnocythere faceta, L. subhubeiensis, Candona* sp., *C. imparilis, Moenocypris* sp., *Potamocypris reticulata*. 3: *Hornichara tornata, H. kasakstanica, Charites minutissina, Nemegtichara brevicylindrica, Sphaerochara minheensis, S. chuankouensis, S. parvula, Pseudolatochara globula, P. pinnacle, P. aechma, P. rhombica* var. *minheensis, Nemegtichara* var. *minheensis, Gyrogona qianjiangica, Grovesichara minheensis, Qinghaichara* sp., *Maedlerisphaera chinensis, M. paraovat, Raskyaechara* sp., *R. subcylindrica, Grambastichara tornata*. 5: *Chenopodipollis, Piceapollenites, Ulmipollenites, Quercoidites, Ephedripites (D, E), Labitricolpites, Betulaepollenites, Meliaceoidites,* Pinaceae, *Tricolporopollenites, Cedripites, Abietineaepollenites, Pinuspollenites, Rhoipites, Celtispollenites, Scabiosapollenites, Tricolpopollenites, Tsugaepollenites, Ginkgo, Cycas,* Rosaceae, Euphobiaceae, *Magnolia, Retitricolpites,* Polypodiacea.
	EOCENE	Honggou		Gray and red gypsiferous mudstone interbedded with muddy gypsum.	1: *Cyprinotus* sp., *C. cevato formis, Limnocythere* sp., *L. subhubeiensis, L. linguida, L. hubeiensis, Candona* sp., *Eucypris* (?), *E. pengzhenensis, Ilyocypris bradyi, I. gibba, I. errabundis*. 3: *Gyrogona qianjiangica, Sphaerochara minheensis, Pseudolatochara pinnacle, P. aechma, P. rhombica* var. *minheensis, P. globula, Charites minutissina, Maedlerisphaera chiensis, Grovesichara minheensis*. 5: *Quercoidites, Meliaceoidites, Ephedripites, E. (E), Celtis, Iodes, Ulmipollenites, Tricolporopollenites, Tricolpopollenites, Proteacidites, Pterisisporites*.
	PALEOCENE	Qijiachuan Fm.	Lower Xining Gp.[a]	Variegated muddy gypsum with interbedded calcareous mudstone. Basal pebbly sandstone.	1: *Limnocythere* sp., *L. linguida, L. hubeiensis, Cyprois* sp., *C. longzhigouensis, Cyprinotus* sp., *C. paradoxus, Ilyocypris* sp., *Cypris* sp., *C. decorosa, C. decaryi, C.* cf. *decaryi, C. deltoidea, C. constans, C. semiobiculata, Eucypris* sp. 3: *Stephanochara breviovalis, S.*cf. *kiangsuensis, Neochara squalida, Peckichara serialis, Rhabdochara kisgyonensis, Sphaerochara parvula, Harrisichara minoriquadsrata, H. yunlongensis*. 5: *Polypodiaceoisporites, P. undulatus, P. triangutus, Ephedripites (D, E), E. (D) trinata, Echitriporites, E. trianguliformis, E. magnus chinatus, Parcisporites, Quercoidites, Ulmipollenites, Pterisisporites, Scabiosapollis, Parviprojectus, Laricoidites, Myrtaceidites, Ulmoideipites krempii, U. tricostams, Momipites coryloides, Beaupreaidites, Nevesisporites, Dolypodiaceoisporites, Schizaeoisporites, Phylbcladidites paleocenicus, Cranwellia, Proteacidites, P. echinatus, Normapollis, Retitricolpites,* Pinaceae, *Symplocosporites, Triprozectus, Rhorpites, Rutaceaepollenites, Sapindaceidites, Phylochadus, Cedripites, Araiucarucariacites, Polypodiaceoidites, Volubilis, Acrostichiam, Woodsia, Hymenophyllumsporites*.
CRETACEOUS	UPPER C.	Minhe Gp.		Red siltstone with interbedded gypsum and mirabilite. Basal sandy conglomerate.	1: *Cristocypridea* sp., *C. latiovata, C. megalabiata, C. didymolabiata, C. amoena, C. primistina, Eucypris* sp., *E. debiloides, E. minheensis, E. qinghaiensis, Cypridea (Cypridea) cavernosa, C. (Pseudocypridina) longa, C. (P.) gigantea, C. (Morinina) xindianensis, C. (Sebastianites) tumida, Candona hupehensis, Talicypridea reticulata, T. amoena, T. laliovata*. 3: *Grambastichara tenuis, G. communis, Latochara yuananensis, L. curtula, Pseudolatochara jianghanensis, P. rhombica, Obtusochara tenuiconica, Sphaerochara parvula, Gyrogona hubeiensis, Charites guanpingensi*. 5: *Gleicheniidites, Osmundacidites, Schizaeoisporites, Classopollis, Ephedripites (D), Tricolporopollenites*.
	LOWER CRETACEOUS	Hekou Gp.	Shangyan Fm.	Red sandstone with interbedded siltstone and thin-bedded gypsum. Mogou and Chela Fms: red conglomerate, sandstone, and siltstone.	Shanyang Formation: 1: *Cypridea (Cypridea) sanmachiensis, C. (C.) deflecta, Cypridea (Bisulcocypridea) skeeteri, Cypridea (Ulwellia) chuankouensis, Rhinocypris* sp., *R. ventriconcava, R. jurassica jurassica, Ziziphocypris costata, Candoniella candida, Djungarica ventrimarcida, Paracyprinotus* spp., *Darwinula* sp. 5: *Piceaepollenites, Cedripites, Classopollis, Ginkgo, Monosulcites, Deltoidospora, Densoisporites, Verrucosisporites, Inaperturopollenites*. Mogou and Chela Formations (Dangchang basin)[c]: 5: *Cyathidites* sp., *C. minor coup, Toroisporites* sp., *Triporoletes* sp., *T. reticulosus, Lygodiumsporites* sp., *L. japanicliforme, L. microadriensis, Leptolepidites* sp., *Reticulitriletes* sp., *Neoraistrickla* sp., *Verrucosisporites* sp., *Apiculatisporites* sp., *Contignispori tes multimuratus, Cicatricosisporites* sp., *Schizaeoisporites certus, Inaperturopollenites* sp., *Psophosphaera* sp., *Callialasporites* sp., *C. trilobatus, C. monoalasporites, Quadraeculina anellaeformis Maljavkina, Q. limbata Maljavkina, Podocarpidites spp., P. scaber, Caytonipollenites spp., Pristinuspollenites bibulbus Bolkhovitina, Parvisaccites* sp., *Jiaohepollis annulatus, Cedripites minutulus krutzsch, Classopollis spp, Aequitriradites* sp., *Piceaepollenites* sp. 6: *Sphaerium* cf. *Shantungensis* Grabau, S. cf. *retigeolosum* Gu et Yu. 7: *Viriparus* cf. *yumenensis* Guo.
			Xiayan Fm.	Red and yellow siltstone and sandstone with interbedded gray shale. Basal pebbly sandstone and conglomerate.	1: *Cypridea* sp., *C. curtarostrata, C.* cf. *triangula* Liu, *C. (Cypridea) unicostata, C. (C.) vitimensis, C. (Ulwellia) koskulensis, C. (U.) meneveensis, C. (U.) chuankouensis, C. (U.) prolixa, C. (U.) prostata, Shouchangensis, Ziziphocypris* sp., *Damonella jiandeensis, Limnocypridea* sp., *Lycopterocypris infantilis, L. flaccida, Rhinocypris ferox, R. jurassica jurassica*. 2: *Yanjiestheria* spp., *Eosestheria qingtanensis, E. xiningensis*. 3: *Mesochara stipitata, M. xuanziensis, Flabellochara jurongica, F.*cf. *jurongica* Z. Wang et Zhang, *Aclistochara stipitata, A. laiae, A. huangshuiensis*. 5: *Deltoidospora, Schizaeoisporites, Piceaepollenites, Classopollis, Inaperturopollenites, Ginkgoretecfina, Cycadopites, Cicatricosisporites, Monosulcites, Eucommidites, Toroisporis, Cyathidites* Minor, *Psophospnaera, Plicatella*.
JURASSIC	UPP. J.[c]	Datonghe Fm.[c]		Red sandstone and brown siltstone. Basal conglomerate.	1: *Damonella huangshuiensis, D. ovata, Jingguella hutouyaiensis, J. ovata, Prelimnocythere pingua, Djungarica ovalis, Darwinula oblonga, Ousocypris area, Minheella minheensis, M. ligulata, M. plicata, M. surita, Lycopterocypris eggeri*. 3: *Minhechara columelaris, Multispirochara subovalis, Mesochara paragranulifera, M. ammoena, Nodosoclavator qinghalenensis, Forochara maedleri, Aclistochara datongheensis, A. bransoni, A. xiangtangensis, A. platyglobata, A. obovata, A. yunnanensis*. 5: *Densoisporites, Classopollis, Callialasporites, Piceaepollenites, Cedripites, Aracucariacites, Perinopollenites, Ischyosporites, Lygodiumsporites, Concavissimisporites, Cicatricosisporites, Schizaeoisporite s*.
	MIDDLE J.	Xiangtang		Red and gray mudstone and sandstone.	1: *Darwinula remua, D. paracontracta, D.* aff. *agitabilis* Jiang, *Lycopterocypris* sp. 3: *Aclistochara minina, A. nuguishanensis, A. brevis, A. platyglobata, Latochara xiaoxiaensis, L. huang zhongensis*.
		Yaojie		Variegated gray-green mudstone with thin beds of black coal.	1. *Darwinula sarytirmenensis, D. xiaoxiaensis, D. discripta, D. comasa* sp., *Metaeypris catenularia, M. maekerrowi*. 2: *Euestheria* cf. *ziliujingensis* Chen. 3: *Aclistochara nuguishanensis, A. brevis, A. xiaoxiaensis, A. xiningensis, A. minima, A.* cf. *jonesi* Deck, *A. spharica*. 4: *Cryptodira* indet. 5: *Deltoidospora, Cyathidites, Lycopodiacidites, Osmundacidites, Obtusisporis, Quadraeculina, Piceaepollenites, Protopinus, Protoconiferus, Psophosphaera, Classopollis, Callialasporites, Cerebropollenites, Kraeuselisporites, Concavissimisporites, Pinuspollenites, Cycadopites*.

Figure 4. Detailed stratigraphic synthesis, lithologic description, and fossil data for the Xining-Minhe and Dangchang basins, compiled from *QBGMR* [1985], *Zhai and Cai* [1984], *Hao* [1988], and *Yu et al.* [2001]. All stratigraphic designations from *QBGMR* [1985], except footnote a, *Zhai and Cai* [1984]; footnote b, *Hao* [1988]; footnote c, *QBGMR* [1991]; and footnote d, *GBGMR* [1988].

B04402

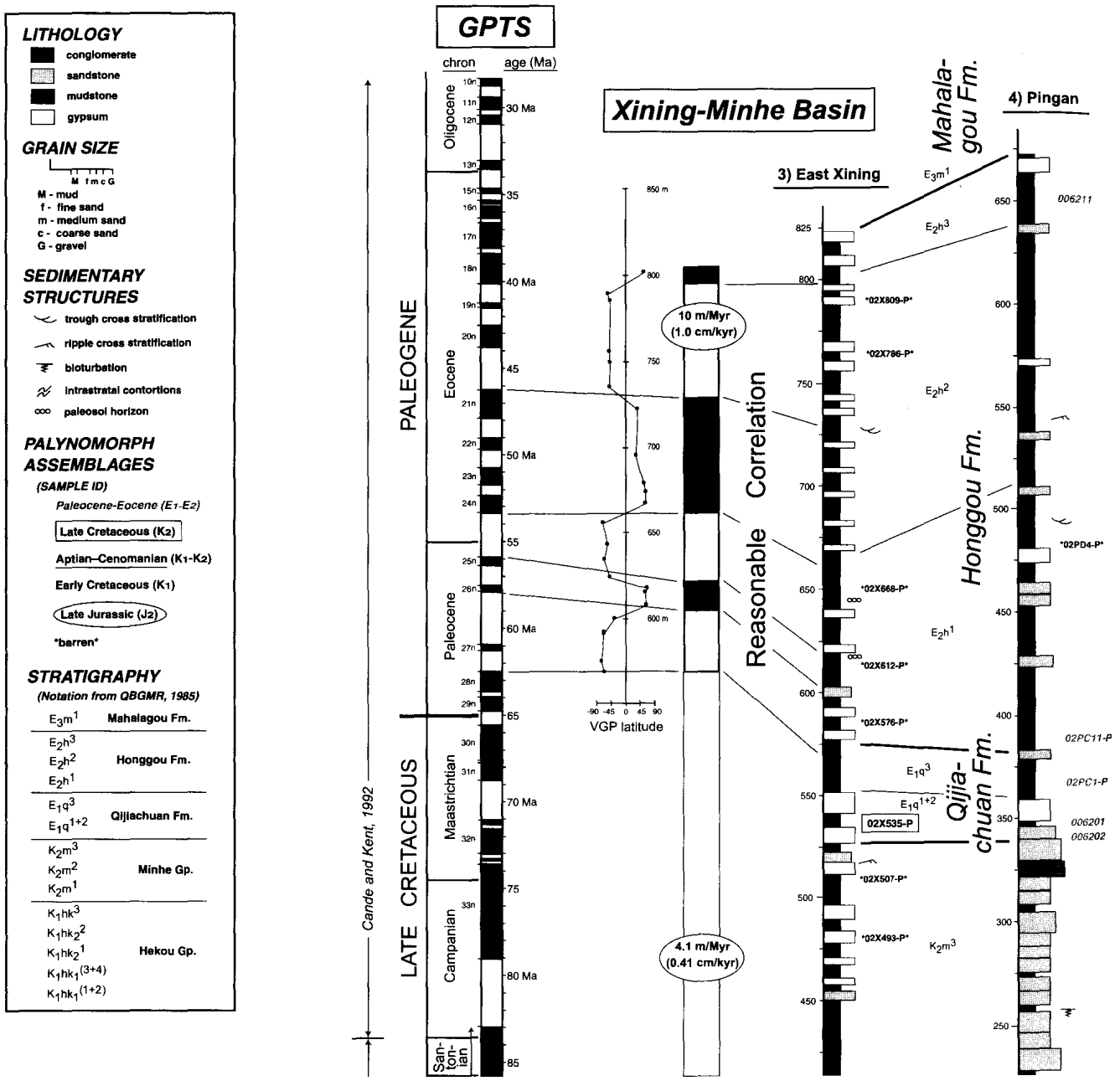

Figure 5. Magnetic polarity stratigraphy and measured sections for the Xining-Minhe and Dangchang basins. Correlations to the geomagnetic polarity timescale (GPTS) utilize age data from 24 palynological assemblages. VGP, virtual geomagnetic pole. Average sediment accumulation rates (undecompacted) are shown for each correlation. Section locations are shown in Figure 2.

bank fluvial setting, with minor overprinting by pedogenic processes.

[16] Proximal fluvial deposits, most common in the southern and eastern portion of the Xining-Minhe basin, compose stratigraphic intervals 10–200 m thick containing medium- to thick-bedded, moderate to poorly sorted, red and tan sandstone and sandy conglomerate. These deposits represent sedimentation by bars and dunes within erosive fluvial channels.

[17] Alluvial fan deposits, best developed in the Dangchang basin and southeastern Xining-Minhe basin, define stratigraphic intervals 20–400 m thick consisting of medium- to thick-bedded, poorly sorted, clast-supported red conglomerate and interbedded sandstone. These strata recorded gravel and sand deposition by fluid flood flows, hyperconcentrated flows, and rare debris flows.

4. Magnetostratigraphy

4.1. Paleomagnetic Sampling and Analysis

[18] Sampling for magnetic polarity stratigraphy was carried out in the central Xining-Minhe basin (east Xining section: 36°35′N, 101°54′E) and Dangchang basin (north Dangchang section: 34°05′N, 104°28′E) (Figure 2). Regionally, these localities afford the most continuous exposure of suitable fine-grained lithologies, greatest palynological age

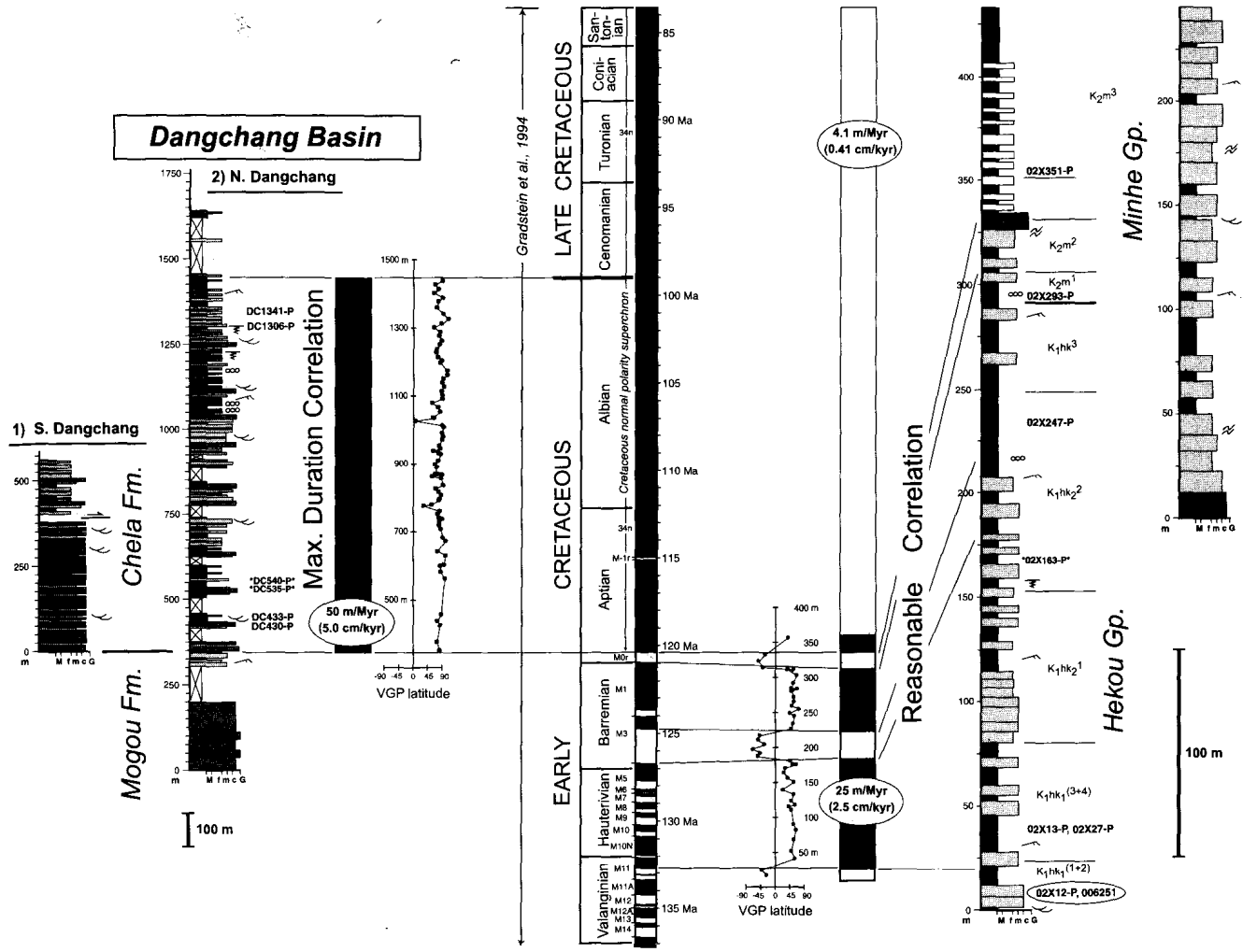

Figure 5. (continued)

control, and greatest structural integrity. Sampling was performed in situ using a portable, gasoline-powered drill. Two to four samples were collected per magnetostratigraphic level (each level representing a horizon <1.0 m thick) at an average stratigraphic spacing of ~10 m. Red mudstone and sandstone were sampled preferentially where possible. A total of 171 magnetostratigraphic levels were collected: 93 Dangchang levels and 78 Xining levels. Magnetostratigraphic sampling was complemented by the regional paleomagnetic study of *Dupont-Nivet et al.* [2004], wherein data tables and complete descriptions of paleomagnetic analyses and thermal demagnetization techniques are provided.

[19] At Dangchang, 85 magnetostratigraphic levels (Figure 5) were collected within a continuous, ~1100-m-thick, southwest dipping homoclinal succession. To perform a fold test, 8 additional paleomagnetic sites (8 samples per site) were collected within strata that are gently folded on a wavelength of several hundred meters and display shallow to moderate (15–34°) westward and northward dips. Upon stepwise thermal demagnetization (~20 temperature steps) of one pilot sample per collected level, 80 of 85 levels yielded interpretable characteristic remanent magnetization (ChRM) directions. Samples from the other five levels, and two additional levels exhibiting aberrant ChRM directions, were discarded from further analysis. Demagnetization behavior is consistent with magnetizations carried by a combination of magnetite and hematite [*Dupont-Nivet et al.*, 2004]. Because normal polarities were obtained from all analyzed levels, no further demagnetization experiments were performed. Therefore each of the calculated virtual geomagnetic pole (VGP) latitudes for the Dangchang section (Figure 5) represents the ChRM direction of a single sample. Positive VGP latitudes were calculated for all levels: the majority are in the 40–80° range, but two (775 and 1025 m levels) exhibit anomalously low values (<25°). The results from these two levels, although suggestive of aberrant readings or local complexities, do not change the interpretation of a single normal polarity zone for the Dangchang section. From the 8 paleomagnetic sites collected to perform the fold test, 8 samples per site were thermally demagnetized and ChRM directions were defined. Site-mean directions cluster after structural correction, indicating passage of the fold test [*McFadden*, 1990] and a prefolding origin for the ChRM [*Dupont-Nivet et al.*, 2004]. A lack of reverse polarities throughout the section precludes application of the reversals test.

[20] The Xining data set (Figure 5) was collected from a continuous, ~800-m-thick, north dipping homoclinal succession that exhibits sufficient variations in bedding attitude suitable for a fold test. Sampling was divided into lower,

intermediate, and upper stratigraphic levels. For the lower section (12–356 m), 55 magnetostratigraphic levels were collected at an average stratigraphic interval of ~6 m. Within intermediate stratigraphic levels (356–553 m), very poorly indurated mudstone and interbedded gypsum prevented sampling. For the upper section (553–801 m), 23 magnetostratigraphic levels were collected at an average stratigraphic interval of ~11 m. For the lower part of the Xining section, 49 of 55 levels yielded interpretable ChRM directions carried mainly by hematite. Three aberrant ChRM directions were discarded. For the remaining 46 levels, ChRM directions pass both the reversals test and the fold test [*McFadden*, 1990; *McFadden and McElhinny*, 1990], consistent with acquisition of the ChRM during or shortly after deposition. For the upper part of the Xining section, 22 of 23 levels yielded ChRM directions carried mainly by magnetite. Although variations in bedding attitudes are insufficient to allow a determinate fold test, the ChRM directions pass the reversals test [*McFadden and McElhinny*, 1990], suggestive of a primary origin for the magnetization.

4.2. Age Correlation

[21] A limited quantity of magnetic polarity zones are defined for the Dangchang and Xining sections, precluding rigorous correlation of polarity zonation to the geomagnetic polarity timescale (GPTS) on the basis of pattern recognition. However, the fossil age data (Figure 4 and Tables A1 and A2) partially restrict possible correlations. Our rationale therefore is to utilize the combination of fossil ages and polarity zonation to define a single reasonable correlation for each section, rather than to match a series of alternative correlations to the GPTS. It must be emphasized that each correlation shown in Figure 5 represents only one of several possible correlations.

[22] For the Dangchang basin, exclusively normal polarities are observed for all 78 magnetostratigraphic levels (350–1437 m level). The uniformity of magnetic polarity, large number of analyzed levels, and ~10 m sampling interval suggest that it is unlikely that significant zones of reversed polarity were missed within the 1087 m sampled interval. Age constraints from new palynological assemblages (433, 596, 1306, and 1341 m levels) consistently indicate an Aptian-Albian (late Early Cretaceous) age (Table A2). Therefore the single, 1087-m-thick, normal polarity zone is correlated to part of the Cretaceous normal polarity superchron (chron 34n). The combination of exclusively normal polarities and Aptian-Albian palynoflora further restrict deposition to a time interval ranging from 120 Ma (base of chron 34n) to 99 Ma (end of Albian), based on the GPTS of *Cande and Kent* [1992] and *Gradstein et al.* [1994]. This 21 Myr window represents the maximum duration for deposition; the possibility of deposition over a shorter time frame cannot be ruled out.

[23] Sampling of the Xining section was divided into lower, intermediate, and upper stratigraphic levels. For lower levels (12–356 m), 36 levels yield normal polarity ChRM directions and reversed polarities are observed at 10 levels. Two normal and three reverse polarity zones are each defined by two or more levels of similar paleomagnetic polarity; a third normal polarity zone at the top of the sampled interval is inferred on the basis of a single level. Eight palynological assemblages (12, 13, 17, 27, 247, 248, 293, and 351 m levels) indicate a Late Jurassic or Early Cretaceous age for the lower Xining section (Table A1). There are many possible correlations of the six polarity zones to the GPTS. In the correlation presented, the Aptian-Cenomanian (121–93 Ma) palynological assemblage at the 351 m level is assumed to lie within the Cretaceous normal polarity superchron (chron 34n of *Cande and Kent* [1992] and *Gradstein et al.* [1994]), which spans from early Aptian (120 Ma) through Santonian (83 Ma). Therefore the stratigraphically highest normal polarity zone, defined by a magnetostratigraphic level at 356 m, is correlated with the lowermost part of chron 34n. Further correlations of underlying polarity zones are as follows: a narrow reversed zone (306–330 m) to chron M0r, a thick normal zone (214–306 m) to chrons M1–M3n, a reversed zone (178–214 m) to chron M3r, a thick normal zone (22–178 m) to chrons M5n–M11n, and the basal reversed zone (12–22 m) to chron M11r of *Gradstein et al.* [1994]. The correlation presented provides a reasonable explanation for the series of palynological assemblages from the lower 400 m of the Xining section, but alternative correlations are possible.

[24] Although paleomagnetic data are not available for intermediate levels (356–569 m) of the Xining section, new palynological assemblages indicate an Aptian-Cenomanian (mid-Cretaceous) age at the 351 m level and a Cenomanian-Maastrichtian (Late Cretaceous) age at the 535 m level (Table A1).

[25] For upper stratigraphic levels (569–801 m) of the Xining section, 22 magnetostratigraphic levels (10 normal polarity, 12 reverse polarity) can be grouped into six polarity zones. Two normal and three reverse polarity zones are each defined by two or more levels of similar polarity; a third normal polarity zone at the top of the sampled interval is inferred on the basis of a single level. However, the wide spacing between magnetostratigraphic levels (a result of limited suitable lithologies) virtually ensures that the observed magnetic polarity zonation will incompletely identify reversals of the GPTS. Utilizing gypsum marker units, new chronostratigraphic data from Paleocene and Eocene palynological assemblages (Table A1) collected nearby at the Pingan section are correlated along strike to the Xining section at the 553, 559, 566, 582, and 865 m levels (Figure 5). A tentative correlation to the GPTS is made wherein the lowest magnetostratigraphic level (569 m) is considered to be near the Cretaceous-Paleocene boundary, based on Late Cretaceous palynoflora at 535 m and Paleocene-Eocene palynoflora at 553–582 m. Further correlations of overlying polarity zones are as follows: a reverse polarity zone (569–604 m) to Paleocene chrons 26r–27r, a normal polarity zone (661–729 m) to early Eocene chrons 21n–24n, and a reverse polarity zone (729–795 m) to middle Eocene reverse chrons 18r–20r. Although offering a reasonable explanation for palynological assemblages, the magnetic polarity correlation presented for the upper Xining section is nonunique. These results are attributable to incomplete sampling of the numerous polarity chrons that characterize the GPTS from Late Cretaceous to Oligocene time.

4.3. Accumulation Rates

[26] Sediment accumulation rates are calculated on the basis of magnetic polarity correlations shown in Figure 5.

All rates discussed here are subject to a host of uncertainties, including the errors in magnetic correlations (mentioned previously), errors in the GPTS, resolution of palynological assemblages, uncertainties related to unsteady deposition and stratigraphic completeness, errors in measured stratal thicknesses, and postdepositional thickness changes [*May et al.*, 1985; *Badgley et al.*, 1986; *Gallagher*, 1989; *McRae*, 1990]. One important issue concerns the possibility of significant time gaps within the stratigraphic successions. Although angular unconformities are not observed, unsteady deposition could result in disconformities of several million years duration (e.g., Jurassic section of Qaidam basin [*Ritts and Biffi*, 2000]). For the Xining succession, the potential for unconformable time gaps is minimized by several factors. First, the upper and lower age bounds indicate a 10^7-10^8 year duration of potential deposition, exceeding the 10^0-10^5 year timescales over which accumulation rates are most sensitive to the effects of unsteady, discontinuous sedimentation [*Sadler*, 1981; *May et al.*, 1985; *Badgley et al.*, 1986; *McRae*, 1990]. Second, the volumetric dominance and large vertical extent of lacustrine facies (Table A3) suggests that (1) erosion of previously deposited sediment, a process common in channelized fluvial systems, was of reduced importance, and (2) deposition was steadier than in a river-dominated system, as demonstrated by *Sadler* [1981]. Third, the paucity of frequent or mature paleosols in overbank (nonchannelized) fluvial deposits suggests, qualitatively and possibly quantitatively [*Kraus and Bown*, 1993; *Retallack*, 1998], that there were not prolonged depositional hiatuses. Additional uncertainties to consider include postdepositional variations in stratal thickness, particularly the effects of compaction. The long-term average rates reported in Figure 5 represent compacted stratigraphic thickness per elapsed time. To remove the effects of compaction beneath younger sedimentary overburdens, a standard backstripping analysis [*Van Hinte*, 1978] was performed assuming reasonable porosity values [*Sclater and Christie*, 1980; *Angevine et al.*, 1990], yielding decompacted rates about 10–30% higher. Given all the possible sources of error, the reported long-term average rates are considered approximations of actual accumulation rates. Significant variations in the actual rates over time frames $<10^6-10^7$ years may remain undetected by the analysis presented here.

[27] For the Dangchang basin, a minimum average rate of 5.0 cm/kyr or 50 m/Myr (55 m/Myr decompacted) during the Early Cretaceous is calculated on the basis of upper and lower age bounds. The termination of basin development is unknown, but deposition persisted into Miocene time in the nearby Nanyang, Niudingshan, and Lixian basins of the western Qinling Shan (Figure 2) [*Zhai and Cai*, 1984].

[28] For the lower Xining-Minhe basin, an average rate of 25 m/Myr (31 m/Myr decompacted) during the Early Cretaceous is calculated on the basis of six polarity chrons. Although intermediate levels of the basin lack paleomagnetic data, underlying and overlying magnetostratigraphic constraints define an average rate of 4.1 m/Myr (5.6 m/Myr decompacted) during Late Cretaceous-early Paleocene deposition. Paleomagnetic data for the upper Xining-Minhe basin incompletely sample polarity chrons of Paleocene-Oligocene strata but the magnetostratigraphic correlation, which is partially restricted by palynomorph assemblages, yields an average rate of 10 m/Myr (13 m/Myr decompacted) for late Paleocene-Eocene time.

5. Discussion

[29] On the basis of magnetic polarity stratigraphy and supporting palynological age data, a plot of age versus stratigraphic thickness (Figure 6) reveals a three-stage history of Mesozoic to mid-Cenozoic sediment accumulation in the Xining-Minhe basin: (1) initial rapid accumulation (Early Cretaceous), (2) substantially reduced accumulation (Late Cretaceous-Paleocene), and (3) renewed rapid accumulation (Paleogene). The Dangchang basin recorded a single phase of rapid accumulation (Early Cretaceous). Calculation of maximum and minimum decompacted thicknesses for the Xining-Minhe basin (based on a variable 500- to 1000-m-thick Oligocene-Miocene overburden and uniform 200-m-thick Pliocene-Quaternary loess) generates an envelope of possible accumulation histories (Figure 6). Total subsidence and tectonic subsidence histories [e.g., *Hendrix et al.*, 1992; *Sobel*, 1999; *Liu et al.*, 2001; *Yin et al.*, 2002] are not calculated due to a lack of independent evidence for surface elevation through time. This reasoning follows *Métivier et al.* [1998] in that accumulation need not be attributed to subsidence, particularly in topographically closed basins. Stages 1–3 of the sediment accumulation history are discussed below.

5.1. Basin Development: Stages 1 and 2

[30] Initial rapid accumulation (Stage 1) followed by decreased accumulation (Stage 2) is attributed to fault-controlled subsidence due to extension and subsequent postrift thermal subsidence. A variety of simple thermal models [*McKenzie*, 1978; *Salveson*, 1978] predict an exponential decay in subsidence rates for several tens of millions of years following a short-lived episode of extension, broadly matching the Cretaceous-Paleocene accumulation pattern for the Xining-Minhe basin (Figure 6).

[31] Paleocurrent data, grain-size trends, and potential basin margin faults are consistent with initial fault-controlled subsidence during Early Cretaceous time. Paleocurrent measurements (Figure 7) of trough cross strata, imbricated clasts, and primary current lineations for the Xining-Minhe basin suggest principal sediment sources to the south and east, consistent with a general coarsening of facies toward the south and east. Two faults displaying normal separation have been mapped in this region (Figure 7) along the southern and eastern margins of the basin: a north dipping fault and west dipping fault, respectively [*QBGMR*, 1985; *Gansu Bureau of Geology and Mineral Resources* (*GBGMR*), 1988]. These faults may form a linked set of faults in a sinistral transtensional setting, similar to the hypothesis of *Vincent and Allen* [1999] for Jurassic-Cretaceous basin development in the Hexi Corridor (Figure 2). Paleocurrents for the Dangchang basin (Figure 7) indicate northeast directed transport, consistent with a profound decrease in grain size from the southwestern limb to northeastern limb of the Dangchang syncline (Figure 5). This dispersal pattern is tentatively attributed to motion along a zone of mapped structures on the southwestern margin of the basin (Figure 7). Further

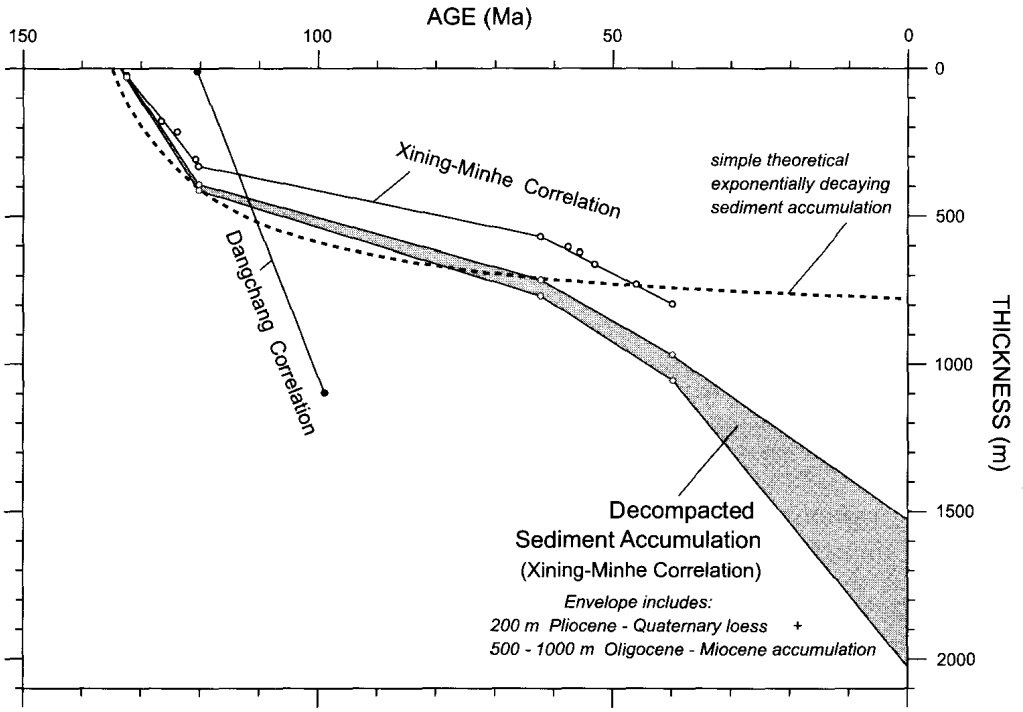

Figure 6. Age versus thickness diagram for stratigraphic sections in the Xining-Minhe basin (open circles) and Dangchang basin (solid circles). Shaded envelope represents decompacted accumulation curve for Xining-Minhe basin (see text). Stratigraphic thickness is plotted with values increasing downward in order to emphasize (1) the time-depth history of the basal stratigraphic level relative to the basin surface (zero thickness level) and (2) the similarity to an exponentially decaying accumulation history (dashed line).

work is needed to assess the original magnitude and sense of slip on this fault system.

[32] Basin development linked to extensional faulting and postrift thermal subsidence can be reconciled with recent thermochronological results for the northern Tibetan Plateau [*George et al.*, 2001; *Jolivet et al.*, 2001; *Sobel et al.*, 2001; *Delville et al.*, 2001; *Cowgill et al.*, 2003]. Although the different data sets suggest slightly different time frames, they consistently indicate rapid Jurassic cooling (either a single cooling episode or series of episodes) and negligible cooling to even minor reheating during Cretaceous time. Minor reheating [e.g., *Jolivet et al.*, 2001] may be the result of burial beneath 1–2 km of Cretaceous synrift and postrift strata.

[33] Structural and stratigraphic evidence also exists for Late Jurassic-Cretaceous extension and related strike-slip deformation in east Asia (Figure 1), notably in the Hexi Corridor [*Xu et al.*, 1989; *Huo and Tan*, 1995; *Vincent and Allen*, 1999], along the Altyn Tagh fault [*Arnaud et al.*, 2003; *Chen et al.*, 2003], on the margins of the Ordos block [*Ritts et al.*, 2001], across Mongolia [*Traynor and Sladen*, 1995; *Johnson et al.*, 2001; *Webb et al.*, 1999; *Graham et al.*, 2001; *Howard et al.*, 2003; *Meng et al.*, 2003], and in northern and eastern China [*Ratschbacher et al.*, 2000; *Davis et al.*, 2001, 2002; *Grimmer et al.*, 2002; *Ren et al.*, 2002; *Zhang et al.*, 2003]. However, coeval Jurassic shortening is defined by thrust structures and associated deposits in the Yinshan belt [*Davis et al.*, 1998], Ordos block [*Ritts et al.*, 2001; *Darby and Ritts*, 2002], eastern Qinling Shan [*Mattauer et al.*, 1985; *Meng and Zhang*, 2000; *Ratschbacher et al.*, 2003], and Mongolia [*Zorin*, 1999]. The driving mechanisms of coeval, or nearly coeval, extension and shortening in neighboring regions, remain poorly understood [*Davis et al.*, 2001; *Graham et al.*, 2001].

5.2. Basin Development: Stage 3

[34] Increased early to mid-Cenozoic sediment accumulation (Stage 3) is revealed by magnetic polarity stratigraphy and palynology for the Xining-Minhe basin, and other regional considerations. An initial increase during Paleogene time was followed by accumulation of a 500- to 1000-m-thick Oligocene-Miocene succession [*QBGMR*, 1985; *GBGMR*, 1988]. Although not directly dated, the magnitude of Oligocene-Miocene deposition requires a further increase in accumulation rates over the Paleogene rates (Figure 6). An extensive Pliocene-Quaternary loess constitutes an additional ~200 m of accumulation [*Sun and Liu*, 2000].

[35] In the northeastern Tibetan Plateau, Oligocene-Quaternary sedimentation persisted in some areas, such as the Xining-Minhe basin (or Xining subbasin), and initiated in new areas such as the Linxia and Lanzhou subbasins and Gonghe, Guide, and Xunhua basins (Figure 2). Numerous studies on Miocene and younger successions, including extensive loess deposits, have recorded a rich mammal biostratigraphic record with well-defined magnetostratigraphic correlations [*Li*, 1995; *Li et al.*, 1997a, 1997b; *Li and Fang*, 1999; *Flynn et al.*, 1999; *Qiu et al.*, 2001; *Yu et al.*, 2001; *Yue et al.*, 2001; *Fang et al.*, 2003; *Pares et al.*, 2003]. Accumulation rates in these successions are markedly higher than early to mid-Tertiary rates. On average, reported Miocene rates are about 20–60 m/Myr [*Li et al.*, 1997a; *Flynn et al.*, 1999; *Li and Fang*, 1999; *Yue et al.*,

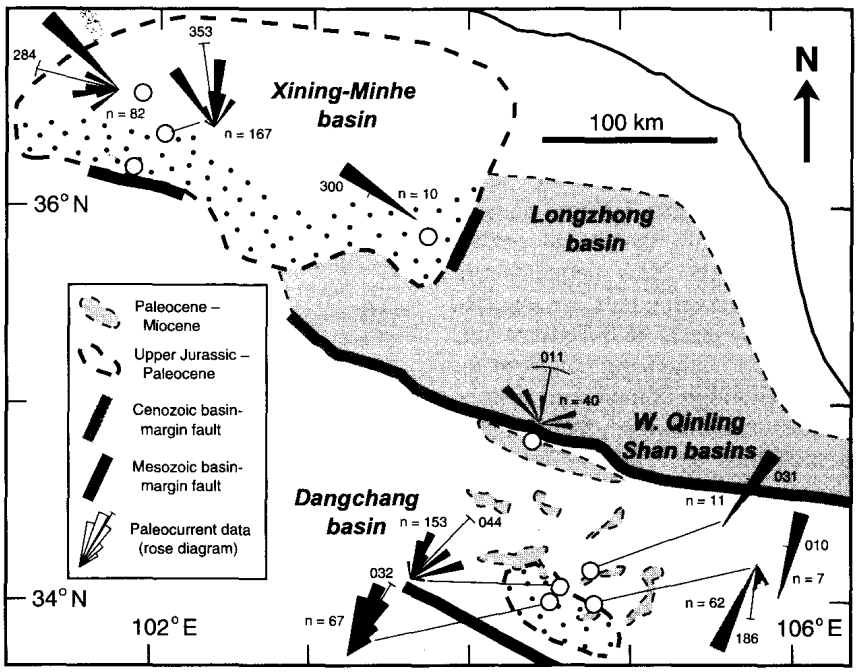

Figure 7. Paleocurrent data and possible basin margin faults related to Mesozoic deposition in the Xining-Minhe and Dangchang basins (black) and Paleogene deposition in the composite Longzhong basin and western Qinling Shan basins (gray). Open circles denote locations of studied stratigraphic sections (shown in Figure 2). Paleocurrent rose diagrams depict vector means and pooled data in 10° bins. Stippled pattern shows the extent of Mesozoic (principally Cretaceous) conglomeratic facies in the Xining-Minhe and Dangchang basins.

2001; *Fang et al.*, 2003] and Pliocene-Quaternary rates are ~200 m/Myr [*Sun and Liu*, 2000; *Pares et al.*, 2003]. Conceivable mechanisms driving this stepwise increase in Cenozoic accumulation rates include (1) increased fault-induced subsidence related to components of normal slip along extensional or strike-slip faults [e.g., *Gaudemer et al.*, 1995; *Hou et al.*, 2003], (2) thrust-related flexural subsidence and generation of accommodation space [e.g., *Horton et al.*, 2002; *Yin et al.*, 2002; *Fang et al.*, 2003], and (3) closure of drainage basin outlets and forced sediment storage [e.g., *Métivier et al.*, 1998; *Tapponnier et al.*, 2001]. Most significantly, the initial increase in accumulation rate coincides spatially and temporally with the regional tectonic (vertical axis) rotation identified by *Dupont-Nivet et al.* [2004]. We suggest that both clockwise rotation and accelerated sediment accumulation at about 40–30 Ma can be attributed to incipient shortening related to the Indo-Asian collision.

[36] Paleocurrent data (Figure 7) are consistent with multiple localized sediment source areas during Cenozoic time. Paleogene strata from the southern Longzhong basin indicate sediment transport from south to north. To the south, relatively small basins in the western Qinling Shan (Figure 7) contain evidence for both south and north directed transport, suggesting diverse local sediment sources. In addition, lateral facies changes and local correlations help define the initial expression of ranges that partitioned the larger Xining-Minhe basin into smaller entities such as the Xining, Lanzhou, Linxia, and Longzhong-Jingning subbasins of the Longzhong basin (Figure 2). Specifically, uplift of two west-northwest striking ranges can be evaluated: the Laji Shan (south of Xining) and the Maxian Shan (south of Lanzhou). The Cretaceous Hekou and Minhe groups can be confidently correlated across these ranges. In contrast, Eocene-Oligocene strata are well developed north of the Laji Shan in the Xining subbasin but absent south of the range, where deposition commenced during Miocene time in the Gonghe, Guide, and Xunhua basins [*Pares et al.*, 2003]. Similarly, initial expression of the Maxian Shan during roughly mid-Tertiary time is evidenced by contrasting Oligocene-Miocene lithofacies systems to the north and south of this range. Progressive compartmentalization of these <30,000 km^2 basins by compressional and transpressional range uplift may provide a conceptual analogue for Cenozoic partitioning of the >100,000 km^2 basins of the Qaidam and Qilian Shan regions [*Bally et al.*, 1986; *Meyer et al.*, 1998].

[37] Published thermochronological data support this history of localized Tertiary rock uplift. Evidence for Eocene-Miocene cooling is present in piecemeal fashion from the western Tarim basin, Altyn Tagh region, and Qilian Shan [*Sobel and Dumitru*, 1997; *Mock et al.*, 1999; *George et al.*, 2001; *Jolivet et al.*, 2001; *Sobel et al.*, 2001; *Cowgill et al.*, 2003]. Tertiary cooling ages occur in smaller proportions and in more restricted regions than the regionally extensive Jurassic cooling ages, consistent with local range uplift during Tertiary time. On the basis of the accumulation rates, thermochronological data, and possible age of seismically imaged growth strata in the Qaidam basin [*Bally et al.*, 1986], these localized uplifts may have initiated as early as ~40 Ma and are reasonably attributed to shortening induced by the Indo-Asian collision. We propose that range uplift in Paleogene compressional and transpressional settings generated sufficient topographic loads to generate new flexural basins and drive renewed subsidence in preexisting basins, although sediment ponding due to closure of drainage

outlets may have accentuated this process [*Métivier et al.*, 1998; *Tapponnier et al.*, 2001].

6. Conclusions

[38] Distinguishing Mesozoic from Cenozoic strata remains a fundamental problem in the Tibetan plateau. Paleomagnetic studies combined with fossil age control help restrict possible stratigraphic ages. New magnetostratigraphic and palynological biostratigraphic data are reported for Upper Jurassic-Lower Cretaceous to mid-Tertiary successions in the Xining-Minhe and Dangchang basins of the northeastern Tibetan plateau. Although complete identification of magnetic polarity zones is not realized, the magnetostratigraphic correlations presented are partially restricted by palynological age constraints. Accumulation rates vary from relatively high values during Early Cretaceous time to low values during Late Cretaceous-Paleogene time, consistent with regional thermochronological and structural evidence for Late Jurassic-Early Cretaceous extension and Late Cretaceous-Paleogene postrift thermal subsidence. Renewed increases in accumulation rates in the Xining-Minhe basin during early to mid-Tertiary time require an additional, younger mechanism of basin subsidence. Published thermochronological evidence for exhumation of localized ranges and regional paleomagnetic evidence for a vertical axis clockwise rotation at 40–30 Ma [*Dupont-Nivet et al.*, 2004] suggest that flexural subsidence related to individual range uplifts drove increased early to mid-Tertiary accumulation in the northeastern Tibetan Plateau during the initial Indo-Asian collision.

[39] **Acknowledgments.** Funding provided by American Chemical Society (Petroleum Research Fund) grant PRF-37207-G8 (Horton), National Science Foundation grant EAR-0106677 (Horton), and a Geological Society of America research grant (Dupont-Nivet). We thank Huihua Zhang and Xiaowei Jiang (Chinese Academy of Sciences, Institute of Geochemistry, Guangzhou) for logistical and field assistance. Comments by Randy Enkin, Bradley Ritts, and an anonymous reviewer improved the manuscript.

References

Allègre, C. J., et al. (1984), Structure and evolution of the Himalayan-Tibet orogenic belt, *Nature*, *307*, 17–22.

Angevine, C. L., P. L. Heller, and C. Paola (1990), *Quantitative Sedimentary Basin Modeling*, *Cont. Educ. Course Note Ser.*, vol. 32, 133 pp., Am. Assoc. of Pet. Geol., Tulsa, Okla.

Arnaud, N., P. Tapponnier, F. Roger, M. Brunel, U. Scharer, W. Chen, and Z. Xu (2003), Evidence for Mesozoic shear along the western Kunlun and Altyn-Tagh fault, northern Tibet (China), *J. Geophys. Res.*, *108*(B1), 2053, doi:10.1029/2001JB000904.

Badgley, C., L. Tauxe, and F. L. Bookstein (1986), Estimating the error of age interpolation in sedimentary rocks, *Nature*, *319*, 139–141.

Bally, A. W., I. M. Chou, R. Clayton, H. P. Eugster, S. Kidwell, L. D. Meckel, R. T. Ryder, A. B. Watts, and A. A. Wilson (1986), Notes on sedimentary basins in China: Report of the American Sedimentary Basins Delegation to the People's Republic of China, *U. S. Geol. Surv. Open File Rep.*, *86-237*, 108 pp.

Burchfiel, B. C., and L. H. Royden (1991), Tectonics of Asia 50 years after the death of Emile Argand, *Eclogae Geol. Helv.*, *84*, 599–629.

Burchfiel, B. C., P. Zhang, Y. Wang, W. Zhang, F. Song, Q. Deng, P. Molnar, and L. Royden (1991), Geology of the Haiyuan fault zone, Ningxia-Hui autonomous region, China, and its relation to the evolution of the northeastern margin of the Tibetan Plateau, *Tectonics*, *10*, 1091–1110.

Burg, J. P., and G. M. Chen (1984), Tectonics and structural zonation of southern Tibet, China, *Nature*, *311*, 219–223.

Burg, J. P., F. Proust, P. Tapponnier, and G. M. Chen (1983), Deformation phases and tectonic evolution of the Lhasa block (southern Tibet, China), *Eclogae Geol. Helv.*, *76*, 643–665.

Cande, S. C., and D. V. Kent (1992), A new geomagnetic polarity time scale for the Late Cretaceous and Cenozoic, *J. Geophys. Res.*, *97*, 13,917–13,951.

Chen, X., A. Yin, G. E. Gehrels, E. S. Cowgill, M. Grove, T. M. Harrison, and X. F. Wang (2003), Two phases of Mesozoic north-south extension in the eastern Altyn Tagh range, northern Tibetan Plateau, *Tectonics*, *22*(5), 1053, doi:10.1029/2001TC001336.

Clark, M. K., and L. H. Royden (2000), Topographic ooze: Building the eastern margin of Tibet by lower crustal flow, *Geology*, *28*, 703–706.

Cogné, J. P., N. Halim, Y. Chen, and V. Courtillot (1999), Resolving the problem of shallow magnetizations of Tertiary age in Asia: Insights from paleomagnetic data from the Qiangtang, Kunlun, and Qaidam blocks (Tibet, China), and a new hypothesis, *J. Geophys. Res.*, *104*, 17,715–17,734.

Cowgill, E., A. Yin, T. M. Harrison, and X. F. Wang (2003), Reconstruction of the Altyn Tagh fault based on U-Pb geochronology: Role of back thrusts, mantle sutures, and heterogeneous crustal strength in forming the Tibetan Plateau, *J. Geophys. Res.*, *108*(B7), 2346, doi:10.1029/2002JB002080.

Darby, B. J., and B. D. Ritts (2002), Mesozoic contractional deformation in the middle of the Asian tectonic collage: The intraplate Western Ordos fold-thrust belt, China, *Earth Planet. Sci. Lett.*, *205*, 13–24.

Davis, G. A., C. Wang, Y. Zheng, J. Zhang, and G. E. Gehrels (1998), The enigmatic Yinshan fold-and-thrust belt of northern China: New views on its intraplate contractional styles, *Geology*, *26*, 43–46.

Davis, G. A., Y. Zheng, C. Wang, B. J. Darby, C. Zhang, and G. Gehrels (2001), Mesozoic tectonic evolution of the Yanshan fold and thrust belt, with emphasis on Hebei and Liaoning provinces, northern China, *Mem. Geol. Soc. Am.*, *194*, 171–197.

Davis, G. A., B. J. Darby, Y. D. Zheng, and T. L. Spell (2002), Geometric and temporal evolution of an extensional detachment fault, Hohhot metamorphic core complex, Inner Mongolia, China, *Geology*, *30*, 1003–1006.

DeCelles, P. G., D. M. Robinson, and G. Zandt (2002), Implications of shortening in the Himalayan fold-thrust belt for uplift of the Tibetan Plateau, *Tectonics*, *21*(6), 1062, doi:10.1029/2001TC001322.

Delville, N., N. Arnaud, J. M. Montel, F. Roger, M. Brunel, P. Tapponnier, and E. Sobel (2001), Paleozoic to Cenozoic deformation along the Altyn-Tagh fault in the Altun Shan massif area, eastern Qilian Shan, NE Tibet China, *Mem. Geol. Soc. Am.*, *194*, 269–292.

Dewey, J. F., R. M. Shackleton, C. Chang, and Y. Sun (1988), The tectonic evolution of the Tibetan Plateau, *Philos. Trans. R. Soc. London, Ser. A*, *327*, 379–413.

Dupont-Nivet, G., B. K. Horton, R. F. Butler, J. Wang, J. Zhou, and G. L. Waanders (2004), Paleogene clockwise tectonic rotation of the Xining-Lanzhou region, northeastern Tibetan Plateau, *J. Geophys. Res.*, *109*, B04401, doi:10.1029/2003JB002620.

England, P., and M. Searle (1986), The Cretaceous-Tertiary deformation of the Lhasa block and its implications for crustal thickening in Tibet, *Tectonics*, *5*, 1–14.

Fang, X., C. Garzione, R. Van der Voo, J. Li, and M. Fan (2003), Flexural subsidence by 29 Ma on the NE edge of Tibet from the magnetostratigraphy of Linxia basin, China, *Earth Planet. Sci. Lett.*, *210*, 545–560.

Flynn, L. J., W. Downs, N. Opdyke, K. Huang, E. Lindsay, Y. Ye, G. Xie, and X. Wang (1999), Recent advances in the small mammal biostratigraphy and magnetostratigraphy of Lanzhou basin, *Chin. Sci. Bull.*, *44*, 105–118.

Gallagher, K. (1989), An examination of some uncertainties associated with estimates of sedimentation rates and tectonic subsidence, *Basin Res.*, *2*, 97–114.

Galvé, A., A. Hirn, M. Jiang, J. Gallart, B. de Voogd, J. C. Lépine, J. Diaz, Y. Wang, and H. Qian (2002), Modes of raising northeastern Tibet probed by explosion seismology, *Earth Planet. Sci. Lett.*, *203*, 35–43.

Gansu Bureau of Geology and Mineral Resources (GBGMR) (1988), Geologic maps of the Daheba, Dangchang, Lianggongzhen, and Xinhua regions (4 sheets), with regional geologic report (1:50,000 scale), 120 pp., Lanzhou, China.

Gaudemer, Y., P. Tapponnier, B. Meyer, G. Peltzer, S. M. Guo, Z. T. Chen, H. G. Dai, and I. Cifuentes (1995), Partitioning of crustal slip between linked, active faults in the eastern Qilian Shan, and evidence for a major seismic gap, the Tianzhu gap, on the western Haiyuan fault, Gansu (China), *Geophys. J. Int.*, *120*, 599–645.

George, A. D., S. J. Marshallsea, K. H. Wyrwoll, J. Chen, and Y. Lu (2001), Miocene cooling in the northern Qilian Shan, northeastern margin of the Tibetan Plateau, revealed by apatite fission-track and vitrinite-reflectance analysis, *Geology*, *29*, 939–942.

Gradstein, F. M., F. P. Agterberg, J. G. Ogg, J. Hardenbol, P. van Veen, J. Thierry, and Z. Huang (1994), A Mesozoic timescale, *J. Geophys. Res.*, *99*, 24,051–24,074.

Graham, S. A., M. S. Hendrix, L. B. Wang, and A. R. Carroll (1993), Collisional successor basins of western China: Impact of tectonic inheritance on sand composition, *Geol. Soc. Am. Bull.*, *105*, 323–344.

Graham, S. A., M. S. Hendrix, C. L. Johnson, D. Badamagarav, G. Badarch, J. Amory, M. Porter, R. Barsbold, L. E. Webb, and B. R. Hacker (2001), Sedimentary record and tectonic implications of Mesozoic rifting in southeast Mongolia, *Geol. Soc. Am. Bull.*, *113*, 1560–1579.

Grimmer, J. C., R. Jonckheere, E. Enkelmann, L. Ratschbacher, B. R. Hacker, A. E. Blythe, G. A. Wagner, Q. Wu, S. Liu, and S. Dong (2002), Cretaceous-Cenozoic history of the southern Tan-Lu fault zone: Apatite fission-track and structural constraints from the Dabie Shan (eastern China), *Tectonophysics*, *359*, 225–253.

Guan, S. Z. (1988), Palaeocene non-marine ostracods in China, in *Evolutionary Biology of Ostracoda*, edited by T. Hanai, N. Ikeya, and K. Ishizaki, pp. 1147–1161, Elsevier Sci., New York.

Halim, N., J. P. Cogné, Y. Chen, R. Atasiei, J. Besse, V. Courtillot, S. Gilder, J. Marcoux, and R. L. Zhao (1998), New Cretaceous and early Tertiary paleomagnetic results from Xining-Lanzhou basin, Kunlun and Qiangtang blocks, China: Implications on the geodynamic evolution of Asia, *J. Geophys. Res.*, *103*, 21,025–21,045.

Hanson, A. D. (1999), Organic geochemistry and petroleum geology, tectonics and basin analysis of southern Tarim and northern Qaidam basins, northwest China, Ph.D. thesis, 388 pp., Stanford Univ., Stanford, Calif.

Hao, Y. C. (1988), Cretaceous and Palaeogene ostracod biostratigraphy in Xining and Minhe basins of China, in *Evolutionary Biology of Ostracoda*, edited by T. Hanai, N. Ikeya, and K. Ishizaki, pp. 1163–1171, Elsevier Sci., New York.

He, J. D., D. S. Van Nieuwenhuise, and F. M. Swain (1988), Biostratigraphy of Paleogene non-marine Ostracoda from east China, in *Evolutionary Biology of Ostracoda*, edited by T. Hanai, N. Ikeya, and K. Ishizaki, pp. 1153–1161, Elsevier Sci., New York.

Hendrix, M. S., S. A. Graham, A. R. Carroll, E. R. Sobel, C. L. McKnight, B. J. Schulein, and Z. Wang (1992), Sedimentary record and climatic implications of recurrent deformation in the Tian Shan: Evidence from Mesozoic strata of the north Tarim, south Junggar, and Turpan basins, northwest China, *Geol. Soc. Am. Bull.*, *104*, 53–79.

Hendrix, M. S., S. A. Graham, J. Y. Amory, and G. Badarch (1996), Noyon Uul syncline, southern Mongolia: Lower Mesozoic sedimentary record of the tectonic amalgamation of central Asia, *Geol. Soc. Am. Bull.*, *108*, 1256–1274.

Horton, B. K., A. Yin, M. S. Spurlin, J. Zhou, and J. Wang (2002), Paleocene-Eocene syncontractional sedimentation in narrow, lacustrine-dominated basins of east-central Tibet, *Geol. Soc. Am. Bull.*, *114*, 771–786.

Hou, Z. Q., H. W. Ma, K. Zaw, Y. Q. Zhang, M. J. Wang, Z. Wang, G. T. Pan, and R. L. Tang (2003), The Himalayan Yulong porphyry copper belt: Product of large-scale strike-slip faulting in eastern Tibet, *Econ. Geol. Bull. Soc. Econ. Geol.*, *98*, 125–145.

Howard, J. P., W. D. Cunningham, S. J. Davies, A. H. Dijkstra, and G. Badarch (2003), The stratigraphic and structural evolution of the Dzereg Basin, western Mongolia: Clastic sedimentation, transpressional faulting and basin destruction in an intraplate, intracontinental setting, *Basin Res.*, *15*, 45–72.

Hsü, K. J. (1989), Origin of sedimentary basins of China, in *Chinese Sedimentary Basins*, edited by X. Zhu, pp. 207–227, Elevier Sci., New York.

Huo, Y. L., and S. D. Tan (1995), *Exploration Case History and Petroleum Geology in Jiuquan Continental Basin*, 211 pp., Pet. Ind. Press, Beijing, China.

Johnson, C. L., L. E. Webb, S. A. Graham, M. S. Hendrix, and G. Badarch (2001), Sedimentary and structural records of late Mesozoic high-strain extension and strain partitioning, East Gobi basin, southern Mongolia, *Mem. Geol. Soc. Am.*, *194*, 413–433.

Jolivet, M., M. Brunel, D. Seward, Z. Xu, J. Yang, F. Roger, P. Tapponnier, J. Malavieille, N. Arnaud, and C. Wu (2001), Mesozoic and Cenozoic tectonics of the northern edge of the Tibetan Plateau: Fission-track constraints, *Tectonophysics*, *343*, 111–134.

Kapp, P., A. Yin, T. M. Harrison, and L. Ding (2002), Cretaceous-Tertiary deformation history of central Tibet, *Geol. Soc. Am. Abstr. Programs*, *34*, 487.

Kapp, P. A., M. A. Murphy, A. Yin, T. M. Harrison, L. Ding, and J. Guo (2003), Mesozoic and Cenozoic tectonic evolution of the Shiquanhe area of western Tibet, *Tectonics*, *22*(4), 1029, doi:10.1029/2001TC001332.

Kidd, W. S. F., Y. Pan, C. Chang, M. P. Coward, J. F. Dewey, A. Gansser, P. Molnar, R. M. Shackleton, and Y. Sun (1988), Geological mapping of the 1985 Chinese-British Tibetan (Xizang-Qinghai) Plateau Geotraverse route, *Philos. Trans. R. Soc. London, Ser. A*, *327*, 287–305.

Kraus, M. J., and T. M. Bown (1993), Short-term sediment accumulation rates determined from Eocene alluvial paleosols, *Geology*, *21*, 743–746.

Lasserre, C., Y. Gaudemer, P. Tapponnier, A. S. Meriaux, J. Van der Woerd, D. Y. Yuan, F. J. Ryerson, R. C. Finkel, and M. W. Caffee (2002), Fast late Pleistocene slip rate on the Leng Long Ling segment of the Haiyuan fault, Qinghai, China, *J. Geophys. Res.*, *107*(B11), 2276, doi:10.1029/2000JB000060.

Leeder, M. R., A. B. Smith, and J. Yin (1988), Sedimentology, palaeoecology and palaeoenvironmental evolution of the 1985 Lhasa to Golmud Geotraverse, *Philos. Trans. R. Soc. London, Ser. A*, *327*, 107–143.

Li, J. (1995), *Uplift of the Qinghai-Xizang (Tibet) Plateau and Global Change*, 207 pp., Lanzhou Univ. Press, Lanzhou, China.

Li, J., and X. Fang (1999), Uplift of the Tibetan Plateau and environmental changes, *Chin. Sci. Bull.*, *44*, 2117–2124.

Li, J. J., et al. (1997a), Late Cenozoic magnetostratigraphy (11-0 Ma) of the Dongshanding and Wangjiashan sections in the Longzhong Basin, western China, *Geol. Mijnbouw*, *76*, 121–134.

Li, J. J., et al. (1997b), Magnetostratigraphic dating of river terraces: Rapid and intermittent incision by the Yellow River of the northeastern margin of the Tibetan Plateau during the Quaternary, *J. Geophys. Res.*, *102*, 10,121–10,132.

Li, Y. W. (1988), The application of Ostracoda to the location of the non-marine Jurassic-Cretaceous boundary in the Sichuan basin of China, in *Evolutionary Biology of Ostracoda*, edited by T. Hanai, N. Ikeya, and K. Ishizaki, pp. 1245–1260, Elsevier Sci., New York.

Liu, G., and R. Yang (1999), Pollen assemblages of the late Eocene Nadu Formation from the Bose basin of Guangxi, southern China, *Palynology*, *23*, 97–114.

Liu, T., M. Ding, and E. Derbyshire (1996), Gravel deposits on the margins of the Qinghai-Xizang plateau, and their environmental significance, *Palaeogeogr. Palaeoclimatol. Palaeoecol.*, *120*, 159–170.

Liu, Z., C. Wang, and H. Yi (2001), Evolution and mass accumulation of the Cenozoic Hoh Xil basin, northern Tibet, *J. Sediment. Res.*, *71*, 971–984.

Mattauer, M., P. Matte, J. Malavieille, P. Tapponnier, H. Maluski, X. Z. Qin, L. Y. Lun, and T. Y. Qin (1985), Tectonics of the Qinling belt: Build-up and evolution of eastern Asia, *Nature*, *317*, 496–500.

May, S. R., R. F. Butler, and F. A. Roth (1985), Magnetic polarity stratigraphy and stratigraphic completeness, *Geophys. Res. Lett.*, *12*, 341–344.

McFadden, P. L. (1990), A new fold test for palaeomagnetic studies, *Geophys. J. Int.*, *103*, 163–169.

McFadden, P. L., and M. W. McElhinny (1990), Classification of the reversal test in palaeomagnetism, *Geophys. J. Int.*, *103*, 725–729.

McKenzie, D. P. (1978), Some remarks on the development of sedimentary basins, *Earth Planet. Sci. Lett.*, *40*, 25–32.

McRae, L. E. (1990), Paleomagnetic isochrones, unsteadiness, and nonuniformity of sedimentation in Miocene fluvial strata of the Siwalik Group, northern Pakistan, *J. Geol.*, *98*, 433–456.

Meng, Q. R., and G. W. Zhang (2000), Geologic framework and tectonic evolution of the Qinling orogen, central China, *Tectonophysics*, *323*, 183–196.

Meng, Q. R., J. M. Hu, J. Q. Jin, Y. Zhang, and D. F. Xu (2003), Tectonics of the late Mesozoic wide extensional basin system in the China-Mongolia border region, *Basin Res.*, *15*, 397–415.

Métivier, F., Y. Gaudemer, P. Tapponnier, and B. Meyer (1998), Northeastward growth of the Tibet Plateau deduced from balanced reconstruction of two depositional areas: The Qaidam and Hexi Corridor basins, China, *Tectonics*, *17*, 823–842.

Meyer, B., P. Tapponnier, L. Bourjot, F. Métivier, Y. Gaudemer, G. Peltzer, S. Guo, and Z. Chen (1998), Crustal thickening in Gansu-Qinghai, lithospheric mantle subduction, and oblique, strike-slip controlled growth of the Tibet Plateau, *Geophys. J. Int.*, *135*, 1–47.

Mock, C., N. O. Arnaud, and J. M. Cantagrel (1999), An early unroofing in northeastern Tibet? Constraints from $^{40}Ar/^{39}Ar$ thermochronology on granitoids from the eastern Kunlun range (Qianghai, NW China), *Earth Planet. Sci. Lett.*, *171*, 107–122.

Molnar, P., and P. Tapponnier (1975), Cenozoic tectonics of Asia: Effects of a continental collision, *Science*, *189*, 419–426.

Murphy, M. A., A. Yin, T. M. Harrison, S. B. Durr, Z. Chen, F. J. Ryerson, W. S. F. Kidd, X. Wang, and X. Zhou (1997), Did the Indo-Asian collision alone create the Tibetan Plateau?, *Geology*, *25*, 719–722.

Pan, Y. (1993), Unroofing history and structural evolution of the southern Lhasa terrane, Tibetan Plateau: Implications for the continental collision between India and Asia, Ph.D. thesis, 287 pp., State Univ. of N. Y., Albany.

Pang, Q., and R. Whatley (1990), The biostratigraphical sequence of Mesozoic non-marine ostracod assemblages in northern China, in *Ostracoda and Global Events*, edited by R. Whatley and C. Maybury, pp. 239–250, Chapman and Hall, New York.

Pares, J. M., R. Van der Voo, W. R. Downs, M. Yan, and X. Fang (2003), Northeastward growth and uplift of the Tibetan Plateau: Magnetostratigraphic insights from the Guide Basin, *J. Geophys. Res.*, *108*(B1), 2017, doi:10.1029/2001JB001349.

Qinghai Bureau of Geology and Mineral Resources (QBGMR) (1985), Geologic maps of the Duoba, Gaodian, Tianjiazai, and Xining regions (4 sheets), with regional geologic report (1:50,000 scale), 199 pp., Xining, China.

Qinghai Bureau of Geology and Mineral Resources (QBGMR) (1991), *Regional Geology of Qinghai Province*, 662 pp., Geol. Publ. House, Beijing, China.

Qiu, Z. X., B. Y. Wang, Z. D. Qiu, F. Heller, L. P. Yue, G. P. Xie, X. M. Wang, and B. Engesser (2001), Land mammal geochronology and magnetostratigraphy of mid-Tertiary deposits in the Lanzhou Basin, Gansu Province, China, *Eclogae Geol. Helv.*, *94*, 373–385.

Ratschbacher, L., B. R. Hacker, L. E. Webb, M. McWilliams, T. Ireland, S. Dong, A. Calvert, D. Chateigner, and H. R. Wenk (2000), Exhumation of the ultrahigh-pressure continental crust in east central China: Cretaceous and Cenozoic unroofing and the Tan-Lu fault, *J. Geophys. Res.*, *105*, 13,303–13,338.

Ratschbacher, L., B. R. Hacker, A. Calvert, L. E. Webb, J. C. Grimmer, M. O. McWilliams, T. Ireland, S. Dong, and J. Hu (2003), Tectonics of the Qinling (central China): Tectonostratigraphy, geochronology, and deformation history, *Tectonophysics*, *366*, 1–53.

Ren, J., K. Tamaki, S. Li, and J. Zhang (2002), Late Mesozoic and Cenozoic rifting and its dynamic setting in eastern China and adjacent areas, *Tectonophysics*, *344*, 175–205.

Retallack, G. J. (1998), Fossil soils and completeness of the rock and fossil records, in *The Adequacy of the Fossil Record*, edited by S. K. Donovan and C. R. Paul, pp. 133–163, John Wiley, Hoboken, N. J.

Ritts, B. D., and U. Biffi (2000), Magnitude of post-Middle Jurassic (Bajocian) displacement on the central Altyn Tagh fault system, northwest China, *Geol. Soc. Am. Bull.*, *112*, 61–74.

Ritts, B. D., B. J. Darby, and T. Cope (2001), Early Jurassic extensional basin formation in the Daqing Shan segment of the Yinshan belt, northern North China block, Inner Mongolia, *Tectonophysics*, *339*, 239–258.

Robinson, D. M., G. Dupont-Nivet, G. E. Gehrels, and Y. Zhang (2003), The Tula uplift, northwestern China: Evidence for regional tectonism of the northern Tibetan Plateau during late Mesozoic-early Cenozoic time, *Geol. Soc. Am. Bull.*, *115*, 35–47.

Sadler, P. M. (1981), Sediment accumulation rates and the completeness of stratigraphic sections, *J. Geol.*, *89*, 569–584.

Salveson, J. O. (1978), Variations in the geology of rift basins: A tectonic model, *Conf. Proc. Los Alamos Natl. Lab., 7487C*, pp. 82–86, Los Alamos, N. M.

Sclater, J. G., and P. A. F. Christie (1980), Continental stretching: An explanation of the post mid-Cretaceous subsidence of the central North Sea basin, *J. Geophys. Res.*, *85*, 3711–3739.

Sobel, E. R. (1999), Basin analysis of the Jurassic-Lower Cretaceous southwest Tarim basin, northwest China, *Geol. Soc. Am. Bull.*, *111*, 709–724.

Sobel, E. R., and T. A. Dumitru (1997), Thrusting and exhumation around the margins of the western Tarim basin during the India-Asia collision, *J. Geophys. Res.*, *102*, 5043–5063.

Sobel, E. R., N. Arnaud, M. Jolivet, B. D. Ritts, and M. Brunel (2001), Jurassic to Cenozoic exhumation history of the Altyn Tagh range, northwest China, constrained by $^{40}Ar/^{39}Ar$ and apatite fission track thermochronology, *Mem. Geol. Soc. Am.*, *194*, 247–267.

Song, C. H., X. M. Fang, J. P. Gao, J. S. Nie, M. D. Yan, X. H. Xu, and D. Sun (2003), Magnetostratigraphy of Late Cenozoic fossil mammals in the northeastern margin of the Tibetan Plateau, *Chin. Sci. Bull.*, *48*, 188–193.

Su, D., Y. Li, J. Yu, W. Zhang, L. Zhang, R. Pu, and R. Yang (1983), Late Mesozoic biostratigraphy of nonmarine Ostracoda and pollen and spores in China, *Acta Geol. Sin.*, *57*(4), 329–346.

Sun, J., and T. Liu (2000), Stratigraphic evidence for uplift of the Tibetan Plateau between ~1.1 and ~0.9 myr ago, *Quat. Res.*, *54*, 309–320.

Tang, F., Z. X. Luo, Z. H. Zhou, H. L. You, J. A. Georgi, Z. L. Tang, and X. Z. Wang (2001), Biostratigraphy and palaeoenvironment of the dinosaur-bearing sediments in Lower Cretaceous of Mazongshan area, Gansu province, China, *Cretaceous Res.*, *22*, 115–129.

Tapponnier, P., et al. (1990), Active thrusting and folding in the Qilian Shan, and decoupling between upper crust and mantle in northeastern Tibet, *Earth Planet. Sci. Lett.*, *97*, 382–403.

Tapponnier, P., Z. Q. Xu, F. Roger, B. Meyer, N. Arnaud, G. Wittlinger, and J. S. Yang (2001), Oblique stepwise rise and growth of the Tibet Plateau, *Science*, *294*, 1671–1677.

Traynor, J. J., and C. Sladen (1995), Tectonic and stratigraphic evolution of the Mongolian People's Republic and its influence on hydrocarbon geology and potential, *Mar. Pet. Geol.*, *12*, 246–249.

Van Hinte, J. E. (1978), Geohistory analysis—Application of micropaleontology in exploration geology, *Am. Assoc. Pet. Geol. Bull.*, *62*, 201–222.

Vincent, S. J., and M. B. Allen (1999), Evolution of the Minle and Chaoshui Basins, China: Implications for Mesozoic strike-slip basin formation in central Asia, *Geol. Soc. Am. Bull.*, *111*, 725–742.

Wang, X., B. Wang, Z. Qiu, G. Xie, J. Xie, W. Downs, Z. Qiu, and T. Deng (2003), Danghe area (western Gansu, China) biostratigraphy and implications for depositional history and tectonics of northern Tibetan Plateau, *Earth Planet. Sci. Lett.*, *208*, 253–269.

Watson, M. P., A. B. Hayward, D. N. Parkinson, and Z. M. Zhang (1987), Plate tectonic history, basin development and petroleum source rock deposition onshore China, *Mar. Pet. Geol.*, *4*, 205–225.

Webb, L. E., S. A. Graham, C. L. Johnson, G. Badarch, and M. S. Hendrix (1999), Occurrence, age, and implications of the Yagan Onch Hayrhan metamorphic core complex, southern Mongolia, *Geology*, *27*, 143–146.

Xu, W., Y. He, and Y. Yan (1989), Tectonic characteristics and hydrocarbons of the Hexi corridor, in *Chinese Sedimentary Basins*, edited by X. Zhu, pp. 53–62, Elsevier Sci., New York.

Yin, A., and T. M. Harrison (2000), Geologic evolution of the Himalayan-Tibetan orogen, *Annu. Rev. Earth Planet. Sci.*, *28*, 211–280.

Yin, A., et al. (2002), Tectonic history of the Altyn Tagh fault system in northern Tibet inferred from Cenozoic sedimentation, *Geol. Soc. Am. Bull.*, *114*, 1257–1295.

Yin, J., J. Xu, C. Liu, and H. Li (1988), The Tibetan Plateau: Regional stratigraphic context and previous work, *Philos. Trans. R. Soc. London, Ser. A*, *327*, 5–52.

Yu, Q., C. Li, F. Gu, Y. Hou, and K. Zhang (2001), *Regional Geologic Character and Field Mapping in the Northeast Margin of Qinghai-Tibet Plateau in Cenozoic*, 123 pp., Univ. of Geosci. Press, Wuhan, China.

Yue, L., F. Heller, Z. Qui, L. Zhang, G. Xie, Z. Qiu, and Y. Zhang (2001), Magnetostratigraphy and paleoenvironmental record of Tertiary deposits of Lanzhou Basin, *Chin. Sci. Bull.*, *46*, 770–774.

Zhai, Y., and T. Cai (1984), The Tertiary system of Gansu province, *Gansu Geology*, pp. 1–40, People's Press of Gansu, Lanzhou, China.

Zhang, K. J. (2000), Cretaceous paleogeography of Tibet and adjacent areas (China): Tectonic implications, *Cretaceous Res.*, *21*, 23–33.

Zhang, P., B. C. Burchfiel, P. Molnar, W. Zhang, D. Jiao, Q. Deng, Y. Wang, L. Royden, and F. Song (1990), Late Cenozoic tectonic evolution of the Ningxia-Hui autonomous region, China, *Geol. Soc. Am. Bull.*, *102*, 1484–1498.

Zhang, P., B. C. Burchfiel, P. Molnar, W. Zhang, D. Jiao, Q. Deng, Y. Wang, L. Royden, and F. Song (1991), Amount and style of late Cenozoic deformation in the Liupan Shan area, Ningxia autonomous region, China, *Tectonics*, *10*, 1111–1129.

Zhang, P. Z., P. Molnar, and W. R. Downs (2001), Increased sedimentation rates and grain sizes 2–4 Myr ago due to the influence of climate change on erosion rates, *Nature*, *410*, 891–897.

Zhang, X., W. D. Mooney, S. Li, and Y. Duan (2002), Structure of the Tibetan Plateau and the Ordos block, *Eos Trans. AGU*, *83*(47), Fall Meet. Suppl., Abstract S51B-1049.

Zhang, Y., S. Dong, and W. Shi (2003), Cretaceous deformation history of the middle Tan-Lu fault zone in Shandong province, eastern China, *Tectonophysics*, *363*, 243–258.

Zheng, H., C. M. Powell, Z. An, J. Zhou, and G. Dong (2000), Pliocene uplift of the northern Tibetan Plateau, *Geology*, *28*, 715–718.

Zorin, V. A. (1999), Geodynamics of the western part of the Mongolia-Okhotsk collisional belt, Trans-Baikal region (Russia) and Mongolia, *Tectonophysics*, *306*, 33–56.

R. F. Butler, Department of Geosciences, University of Arizona, Tucson, AZ 85721, USA. (butler@geo.arizona.edu)

G. Dupont-Nivet, Faculty of Earth Sciences, Paleomagnetic Laboratory "Fort Hoofdijk", Utrecht University, Budapestlaan 17, 3584 CD Utrecht, Netherlands. (gdn@geo.uu.nl)

B. K. Horton, Department of Earth and Space Sciences, University of California, Los Angeles, CA 90095-1567, USA. (horton@ess.ucla.edu)

G. L. Waanders, 1475 Rancho Encinitas Drive, Encinitas, CA 92024, USA. (waanpaly@cts.com)

J. Wang, Institute of Geochemistry, Chinese Academy of Sciences, Guangzhou 510640, China. (wangjh@gig.ac.cn)

J. Zhou, Faculty of Earth Sciences, China University of Geosciences, Wuhan 430074, China. (zjy522@mail.cug.edu.cn)